Structural and Biophysical Characterization of Prohibitin

Benchmen Choun Trieu

University of Manitoba

A thesis submitted to the Faculty of Graduate Studies in partial

fulfillment of the requirements of the degree of

Master of Science

Department of Chemistry

University of Manitoba

Winnipeg, Manitoba, Canada

Abstract

Prohibitin (PHB) is a multimeric protein found on lipid rafts of the eukaryotic inner-mitochondrial membrane. The protein is comprised of 3 domains: an N-terminal transmembrane helix, a PHB domain found at the center, and followed by a C-terminal coiled-coil domain. PHB has been shown to function as an intracellular signalling mediator in various cellular processes such as iron homeostasis, cell apoptosis, and mitochondrial DNA maintenance. Many of these processes are associated with the diseases that affect the general population ranging from cancer to obesity. Since no atomic resolution structure of PHB is known, such a determination will provide insight towards its function and furthermore the role it plays within the cell as well as the entire organism. X-ray Diffraction is the desired method for structure determination; therefore, preliminary data pertaining to the protein's behaviour in various solvent conditions will facilitate protein crystallization. This study describes biophysical and structural aspects of (PHB1)-25-252-CHis_6 from dynamic light scattering, analytical ultracentrifugation, transmission electron microscopy, and small angle X-ray solution scattering. CD data was used to determine the quality of refolding protein and showed that it was refolded but without functional assays available, it is unknown whether the protein is properly folded. Sedimentation and microscopy results indicate that the protein forms large oligomers. Further scattering and sedimentation data analysis showed that when protein concentrations were increased from 1-60mg/mL, the protein decreases in particle size. This may be due to large protein sizes, normally observed for proteins at greater concentrations, collapsing and forming smaller structures.

Acknowledgements

I would like to thank Dr. Stetefeld, Dr. George Orriss, Dr. Trushar Patel, Dr. Markus Meier for their supervision, guidance, support throughout my time in the lab. I would also like to thank Dr. Suresh Mishra and Dr. Pauline Padilla-Meier for their guidance and help with learning the background of the project. Many thanks go to Natalie Krahn, Aniel Moya Torres, Matthew McDougall, Fraser Farens, Olga Francisco, and the rest of the Stetefeld Research group for their continuous support and helping me get accustomed to graduate studies and biochemistry research.

I also extend my gratitude towards Dr. Timothy Booth and Daniel Beniac from the National Microbiology Lab in Winnipeg, Manitoba for their introduction, help, and interpretation of the transmission electron microscopy results. This paved the way for potential higher resolution experiments to determine structural properties of PHB1 for future studies.

The research would not be possible without the generous financial support from the Natural Sciences and Engineering Research Council (NSERC), Canadian Institutes Health Research, and the University of Manitoba.

Table of Contents

List of Tables

List of Figures

1.0 INTRODUCTION

1.1 PROHIBITIN DISCOVERY

Prohibitin (PHB) was first discovered by McClung (1989) when screening for tumor suppressors in rat liver cells. It was observed that when the gene was introduced to human fibroblast cells, DNA synthesis was inhibited which is important in cell proliferation. [1] Further screening showed inconsistent mRNA expression between various tissues and cell growth rates. Cardiac muscle and brain tissues have low cell growth rates exhibited moderate to high transcription rates. Liver and spleen cells, which have high cell growth rates, were observed to have the lowest level of transcription. Despite the inconsistent transcriptions rates, evidence of expression across a large range of tissues and cell types suggests a gene that played a universal role in DNA synthesis inhibition and cell proliferation. The gene and protein product was named Prohibitin (PHB) due to the observed inhibitory function. [1] Later on, it was discovered that the gene product was not responsible for this but was attributed to the 3'-untranslated region. [2] Despite this, an interest in PHB still remains. Since then, numerous studies have been done to further uncover the physiological roles this protein has in the cell, which will be introduced later. [3] The two homologues of Prohibitin are named PHB1 and PHB2. Less common names for the two homologues are also B-cell receptor associate protein (BAP) 32 and 37, respectively. PHB is found on the inside of the mitochondrial intermembrane, has been shown to be involved in essential cellular processes including mitochondrial biology, intracellular insulin signalling, iron homeostasis, and cell proliferation. [1, 3, 4, 5]

1.2 KNOWN STRUCTURAL CHARACTERISTICS

Some basic structural characteristics of PHB are known. Both homologues of PHB are comprised of 3 domains. An N-terminal region of hydrophobic residues forms a transmembrane domain anchoring the protein on to the membrane. The two remaining domains are exposed to the mitochondrial intermembrane space. A central domain is called the PHB domain. This region is a conserved region with homology to a family of scaffold proteins called the Stomatin-Prohibitin-Flotillin-HflK/C (SPFH) family. The final domain is a C-terminal coiled-coil domain believed to be responsible for the interactions between the two PHB homologues (Figure 1A). [5] These two homologues share more than 50% amino acid residues. [6] Western blot analysis experiments involving yeast mutants with deleted PHB1 or PHB2 genes resulted in loss of detectable levels of the opposing homologue. Expression was restored when synthetic plasmids containing the deleted gene were reintroduced into the yeast cells. This suggested an interdependency between the two homologue of PHB. [7] Back *et al.* (2002), by analyzing cross-linking experiments between the two homologues via mass spectrometry, suggested that *in vivo*, the two PHB homologues form a heterodimer which then assembles into a 1 MDa scale ring-like structure embedded onto the mitochondrial membrane (Figure 1B). Crosslinking was performed on complete PHB complex using lysine reactive crosslinkers, retaining complex integrity during mass spectrometry experiments. [8] Electron microscopic images were collected by Tatsuta *et al*. showing these large rings (Figure 1C). [9] Many predictions have been made for the three-dimensional shape of this ring, one of which is the Vault Shell Model (Figure 2) used for describing the appearance of ribonucleoprotein particles. This structure resembles that of a large hollow dome sitting upon the membrane. The study compared to proteins of the SPFH family such as stomatin of *P. horikoshii* and mouse flotillin-2. With the highly conserved residues

amongst the SPFH proteins, this suggests that the PHB complex might adopt a similar conformation as a hollow dome rooted into the mitochondrial membrane. [10] It is in this conformation that is believe to be responsible for it's cell signalling properties. The large complex is believed to be a "signalling hub" where other proteins such as mAAA-protease and cytrochrome *c* oxidase dock or interact upon contact. [6] Despite what is known about PHB, no experimental evidence exists that truly depict the actual three-dimensional conformations of the individual homologues.

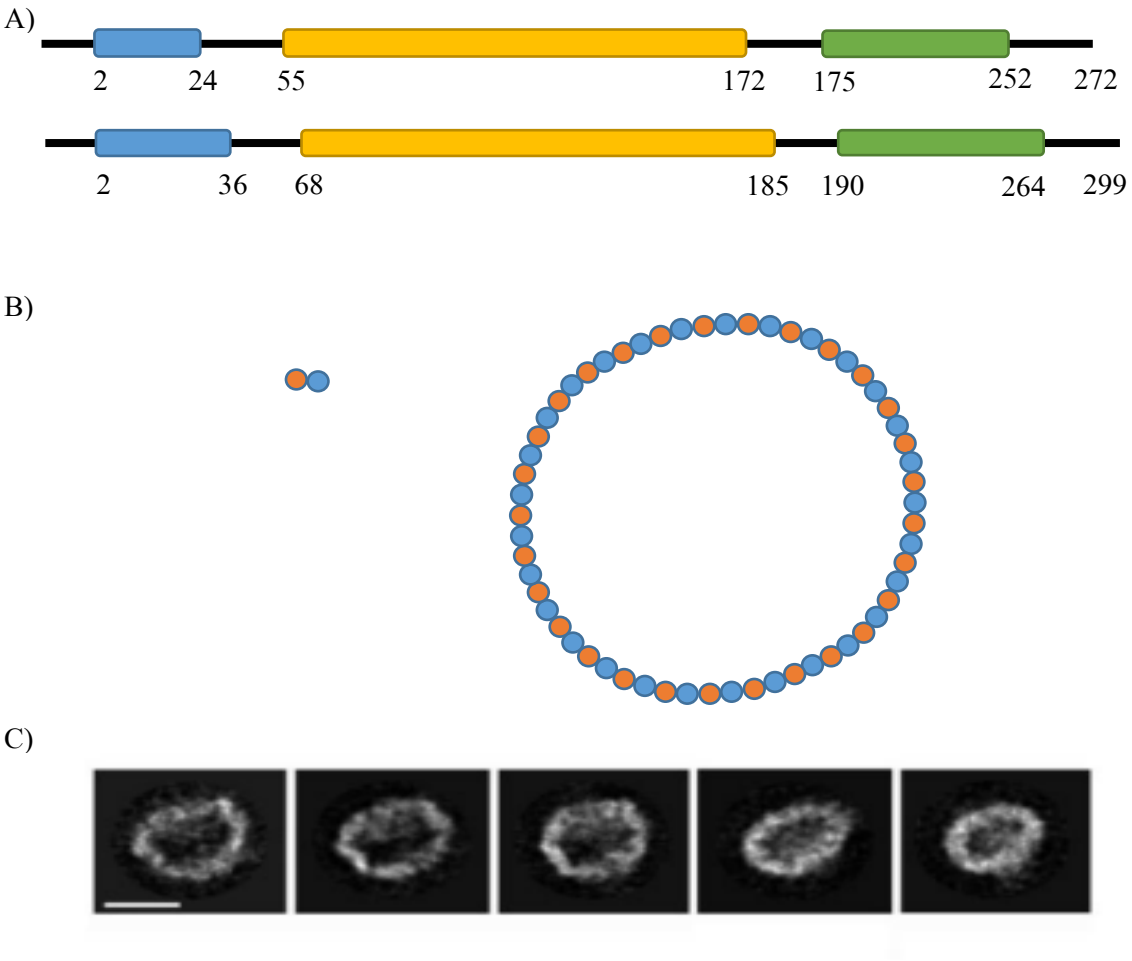

Figure 1: Basic structural aspects of PHB, an adaptation of Back *et al.* [8] A) Illustration of 3 domains of PHB 1 and 2: N-terminal transmembrane domain (blue), PHB domain (yellow), and coiled-coil domain (green). B) Left; Heterodimer of PHB1 (Orange) and PHB 2 (Blue) and right; ring formed by multiple sets of heterodimers. C) Images from single particle electron microscopy (Tatsuta *et al.* 2005). [9]

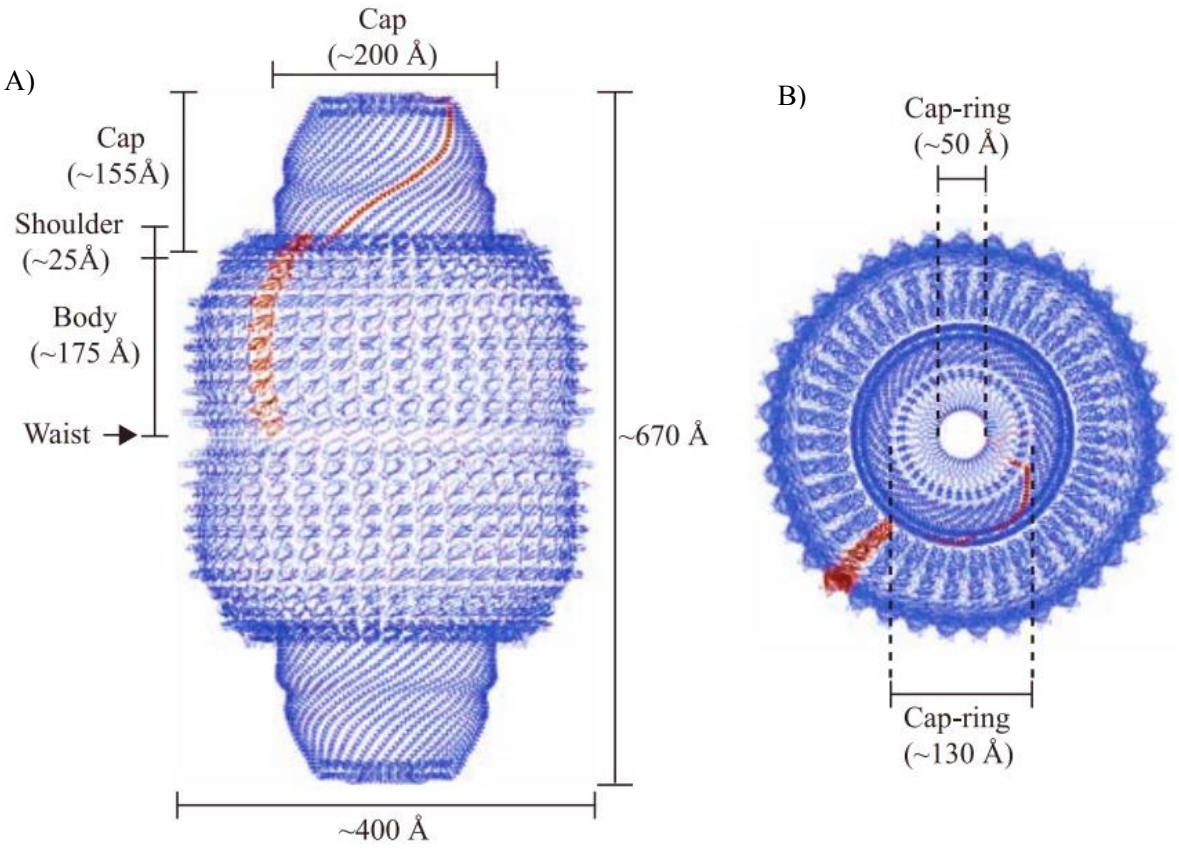

Figure 2: Vault Shell Model as proposed model for PHB structure. [10] A) Side view; PHB would be resemble the shoulder and cap portion sitting upon the inner-mitochondrial membrane forming a dome. B) Top view illustrating ring-like structure.

1.3 PROTEIN FUNCTION

Prohibitin has several functions that are essential in maintaining cell viability. These functions range from mitochondrial maintenance to complex intracellular signalling. PHB has been shown to possibly maintain several functions in the mitochondria such as chaperoning newly synthesized mitochondrial respiratory proteins and more recently maintaining mitochondrial DNA (mtDNA) stability and organization. [3, 4] In addition, a protein that plays an important role in maintaining mitochondrial proteostasis, ATP-dependent m-AAA protease, is believed to interact with the fully assembled PHB ring (Figure 3). In the absence of PHB, m-AAA protease exhibited an increase in activity. Impaired growth was also observed when both PHB and the protease were absent. [11] Nijtmans *et al* reported that Cytochrome *c* oxidases requires the presence of PHB to properly assemble. Cytochrome *c* oxidase, or Complex IV of the electron transport chain, is observed to only assemble from its subunits Cox3p and Cox2p in yeast cells overexpressing PHB1 and 2. [12] Another study demonstrated loss in mtDNA dye-binding in silenced PHB1 mutant cells. HeLa cells transfected with a vector containing a PHB1-interfering RNA gene were stained with a mtDNA stain, PicoGreen. When compared to HeLa cells transfected with a vector not containing the silencing gene, cells containing the interfered PHB1 gene showed decreased mtDNA binding. This suggests a potential mtDNA stabilizing function for PHB1. [13]

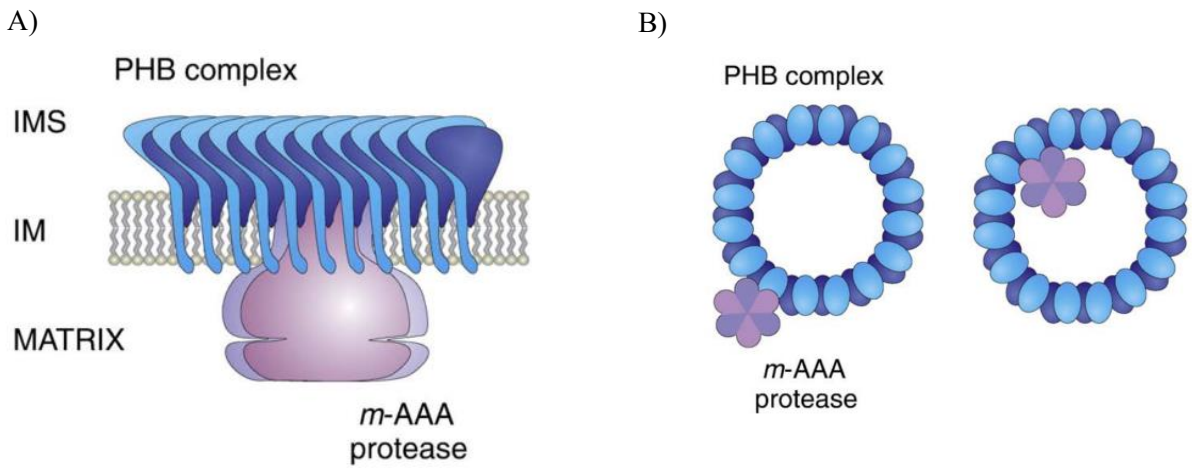

Figure 3: Proposed assembly of the PHB ring and ATP-dependent m-AAA protease in *S. cerevisiae*.[12] Light and dark blue shapes represent PHB monomers and the purple is the protease. A) Side-view alongside the inner-mitochondrial membrane. B) Top view of two probable arrangements of the complex. IMS = intermembrane space, IM, inner-mitochondrial membrane.

Post-translational modifications of proteins play a crucial role in protein structure and function.[14] After various post-translational modifications such as phosphorylation, fatty-acylation, and glycosylation; PHB becomes involved in many signalling and physiological roles.[15] Studies involving phosphorylation of Tyr114 and Thr258 on PHB1 contribute to binding interactions with Shp1/2 and Akt, respectively. Both binding partners are involved in insulin signalling.[16,17] This involvement in insulin regulation may shed light on the development of diabetes and novel remediation for the condition. Although PHB is primarily located on the mitochondrial membrane, it can also be found on the plasma membrane.[18] PHB1 phosphorylation at Thr258 and Tyr259 were observed at higher levels on the plasma membrane of highly invasive cancer cells. This suggests a correlation between phosphorylated membrane-localized PHB1 and the invasiveness of cancer cells.[19] Phosphorylation also occurs at tyrosine residues 114 and 249, in addition to Tyr259 in PHB1. It

is believed that these tyrosine residues are involved in binding iron on the mitochondrial membrane. This gives rise to the possibility that PHB1 and overall PHB might be involved in iron homeostasis when phosphorylated in the mitochondrion, an organelle that extensively uses iron as shuttles for electron transport and energy transduction. [20] Protein fatty acylation is a common occurrence; playing a major role in protein localization and signalling. [21] Cysteine acylation occurs commonly with palmitic acid. [22] Experiments conducted by Ande *et al* suggest that PHB might undergo fatty-acyl post-translational modification at Cys69, with an acyl-palmitate being the addition. [23] The experiment suggests that PHB palmitoylation may play a role in how the protein can interact with lipid raft systems, which are assemblies of various proteins and cell signalling factors in a region of high cholesterol and saturated lipids on the cell membrane. [24, 25] Flotillin-1, a member of the SPFH family of proteins containing a PHB domain, is also palmitoylated near the N-terminus, which is believed to be involved in the protein's possible membrane association. [25]

Although the focus of this project will be on human PHB, the protein has been characterized, functionally, in various other eukaryotes including plants, roundworms, mammals and as previously described for yeast. Unlike in mammals and roundworms which contain only two genes for PHB, plants may have several more as part of their genomes. Four genes with sequences resembling PHB were characterized in maize. [26] However, plant PHB are still involved in similar cellular processes to that of mammals and yeast including growth inhibition and cell death. [27] In roundworms, reduced PHB levels cause inhibited development during embryonic development as seen in mammals. During post embryonic development in roundworms, reduced PHB levels cause infertility and lethality in offspring. [28]

1.4 BRIEF INTRODUCTION TO TECHNIQUES USED DURING PROJECT

Several techniques will be utilized during the course of this project including protein production in inclusion bodies and protein denaturation and refolding. The goal is to characterize PHB1 using dynamic light scattering, analytical ultracentrifugation, small angle X-ray scattering, and transmission electron microscopy.

Many methods are used when attempting to express high levels of recombinant protein. One common method is protein expression as inclusion bodies. Inclusion bodies are produced in *E. coli* and composed of densely packed denatured protein. In order for the protein to be studied, it must be solubilized and refolded. Solubilization requires the use of a denaturant such as urea or guanidine hydrochloride. [29] The reason why urea is able to denature protein at the molecular level is not fully understood. However, it is believed to facilitate the exposure of hydrophobic residues to the solvent by inserting itself in between residues and in hydrophobic cores. This insertion is thought to be responsible for solubilizing hydrophobic residues. [30] Refolding will then involve slowly removing the denaturant and in some cases the presence of reducing agents. Many methods of refolding exist such as dilution, dialysis, and solid-phase refolding but this project will utilize dialysis as it is one of the simplest methods. [29, 31]

Dynamic Light Scattering (DLS) is a non-destructive, spectroscopic technique analyzes a particle's motion in solution. In a solution of constant temperature, proteins in solution experience constant random motion called Brownian motion. When light comes in contact with a solution and the contents of the solution such as protein particles, the light begins to scatter. As the protein tumbles in solution, the scattering will begin to fluctuate depending on the changes in distance between the continuously moving protein. The fluctuation is correlated to a timescale

which can be used to calculate a size distribution and determine a protein's hydrodynamic radius. Larger fluctuations are observed in larger proteins with slower ranges of Brownian motion. Smaller proteins experience quicker motion resulting in smaller fluctuations. Since Brownian motion is intrinsic to a proteins shape and size, sample heterogeneity can be determined. Figure 4 illustrates homogeneous and uniformly sized protein provide a sharper distribution. Therefore, DLS can be used as a method to determine the homogeneity of a protein sample and, to some extent, the propensity to crystallize. [32, 33, 34]

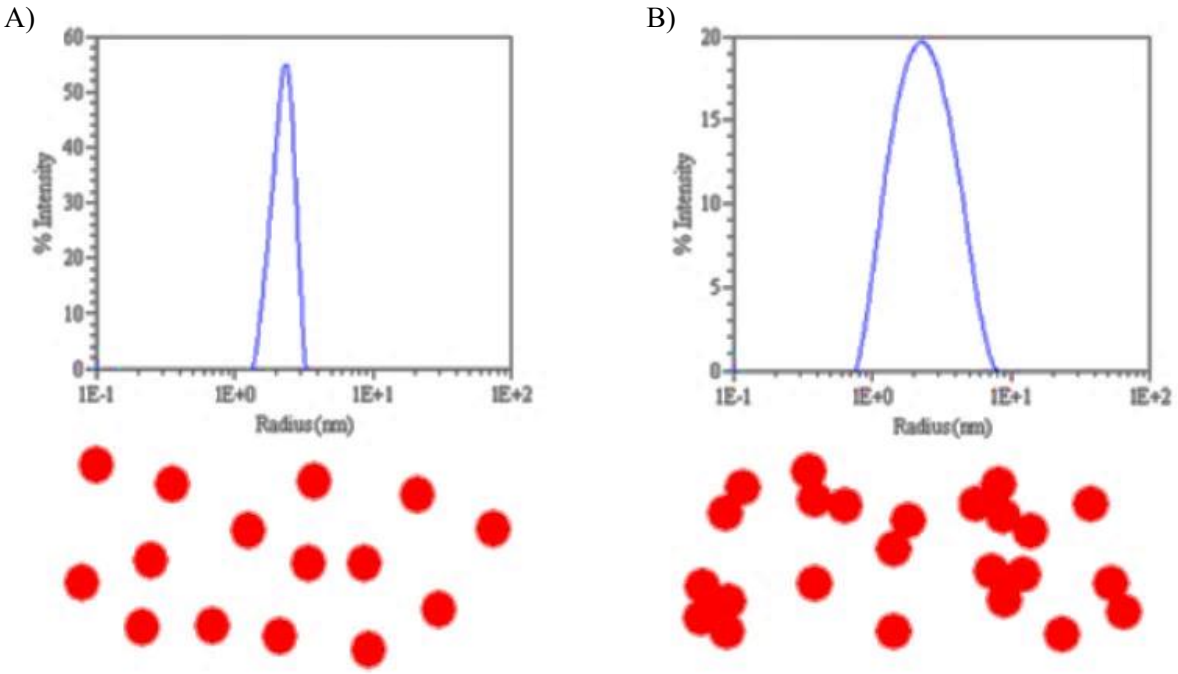

Figure 4: Example DLS plots illustrating differences between homogeneous and heterogeneous protein solution from Arzenšek *et al*. [34] A) Homogeneous solution with particles adopting uniform sizes. B) Heterogeneous solution with particles adopting complexes of different sizes. Multiple peaks may also be observed for heterogeneous solutions (not shown) if differences in sizes are significant.

Analytical Ultracentrifugation (AUC) is another technique used in analyzing proteins in solution. By using a centrifuge equipped with spectrophotometric capabilities, protein sedimentation velocities and sizes can be experimentally determined. During a sedimentation experiment, the proteins experience centrifugal forces due to rotation based on its molecular mass. Larger proteins will proceed to sediment at a greater rate. A protein's sedimentation velocity is proportional to its sedimentation coefficient. Due to this property, it is possible to determine a protein's sedimentation coefficient. In addition to determining a protein's sedimentation, it is possible to determine the stoichiometry of a protein complex. Results that indicate a protein size larger than an expected, may indicated the formation of a multimeric complex. However, the presence of multiple sedimentation peaks may also suggest multiple heterogeneity in a protein sample. [35, 36]

Small angle X-ray scattering (SAXS) is commonly used to determine protein structures in solution at low-resolutions. The method can be used to observe oligomeric protein and various domains of individual proteins. However, SAXS was initially used to determine important protein parameters such as radius of gyration (R_g) and maximum intramolecular distance (D_{max}) which are related to a proteins size. By using these parameters and the scattering profiles of a sample, a three-dimensional representation of the protein can be determined. The D_{max} parameter can be used to develop a pair distribution function to categorize the general shape of the protein. The technique can also be used to assess the how well a protein is folded by creating a Kratky plot. The resulting models are limited to primitive shapes such as spheres, cylinders, or disks, however. Although the method generates lower resolution structures compared to X-ray crystallization and diffraction, it is still considered as a valid technique as it compliments and assists in validating structures determined from other methods. [37, 38]

1.5 PROJECT OBJECTIVE

Decades of research have provided information about the function and basic structure of Prohibitin but none at the molecular level. The knowledge that can be gained regarding the various diseases involving PHB provides the motivation for this project. Thus the focus for this project is to develop a method for producing PHB 1 and 2, in high quality, and uncover structural aspects that may elude to discovering the molecular structure of the protein. Knowledge of the molecular structure will further the understanding of how PHB affects or is affected by those diseases. The preferred method for structure determination will be X-ray diffraction, thus uncovering preliminary structural information may facilitate this or elucidate other methods

2.0 MATERIALS & METHODS

The products of all molecular biology reactions and cloning were visualized and analyzed on 1.5% agarose gels with Hydragreen DNA dye (Actgene, NJ, USA). Proteins were analyzed on 13% SDS-PAGE gels and stained with coomassie brilliant blue (CBB) dye. For all urea-containing buffers, urea solutions were deionized using Bio-Rad AG® 501-X8 (D) resin prior to addition of other buffer components.

2.1 PHB1 PLASMID SYNTHESIS

2.1.1 GENE POLYMERASE CHAIN REACTION (PCR)

All genes created and used were derived from human PHB gene products provided by the Suresh Mishra Group (University of Manitoba). The following procedure was used for PHB1 constructs: 22-252, 28-252, 31-252; and PHB2 36-299. Primers were designed and purchased from Alpha DNA, Canada. PCR reactions were performed using the Stratagene Robocycler Gradient 96 system (Stratagene, USA) with Novagen KOD DNA Polymerase PCR kits and reagents (EMD Millipore, Canada). The reagents and primers were combined as instructed by the kit user manual. The PCR reactions were performed with 30 cycles of 95°C thermal denaturation (30sec), annealing temperatures of ranging from 56-67ºC, with an extension step at 70°C (30sec).

2.1.2 GENE INSERTION AND CLONING

Gene inserts for PHB1 22, 28, 31-252 and PHB2 36-299 were made using PCR (see section 2.2.1). Gene inserts for PHB1 25-252 were obtain from IDT, Canada. The inserts were cloned into pre-restricted pET21a (with NdeI/XhoI) containing an ampicillin (Amp)-resistance gene and C-terminal hexahistidine tag sequence, (His_6). Cloning was conducted using NdeI and XhoI (Thermo Scientific – FastDigest™) for restriction and Quick Ligase (New England Biolabs, U.S.A) for ligation. The plasmids were transformed into Z-competent™ DH5α *E.coli* cells (Zymogen, U.S.A) and plated onto lysogeny broth (LB)/agar/Amp plates, pre-warmed to 37°C. Selected colonies were used to inoculate 3mL LB/Amp media and were incubated at 37°C overnight with constant shaking at 200rpm. Plasmids were isolated and purified using the GeneJET Plasmid Miniprep Kit (Thermo-Scientfic, U.S.A). Samples of the plasmid were restriction digested with NdeI and XhoI to confirm successful gene insertion. Plasmids were also checked for efficacy via commercial sequencing at Manitoba Institute of Cell Biology. Final constructs were named (PHB1)-31(or 22, 28)-252-CHis_6 and (PHB2)-36-299-CHis_6.

2.2 EXPRESSION AND PURIFICATION OF SOLUBLE (PHB1)-31-252-CHis_6

(PHB1)-31-252-C-His_6 was transformed into calcium chloride-competent *E. coli* C41 (DE3) strain cells and plated out onto LB/agar/AMP plates. Colonies were selected and inoculated into 50mL LB pre-culture in the presence of ampicillin. The culture was incubated overnight at 37°C with constant shaking at 200rpm. On the following day, 25mL of the pre-culture was used to start a 500mL LB main culture in the presence of ampicillin. The main culture was incubated at 25°C with constant shaking at 200rpm. Cell cultures were induced with

isopropyl β-D-1-thiogalactopyranoside (IPTG) to a final concentration of 0.4mM once the OD_{600} reaches 0.4. The culture was left to shake incubate for an additional 16 hours (overnight) at 20°C. Cells were collected and pelleted by centrifugation at 6500rpm for 15 mins at 4°C. The pellet was re-suspended and homogenized into 50mM sodium phosphate (Na_2HPO_4), 300mM sodium chloride (NaCl), pH 8.0 (Buffer A) and stored at -20°C in the presence of protease until prepared for lysis. Following cell lysis via french pressing, cellular debris was collected via centrifugation at 25000rpm for 1.5 hours at 10°C. The supernatant was added to HisPur™ Nickel Resin pre-equilibrated with two column volumes of Buffer A. The supernatant-resin mixture was slowly rocked overnight at 4°C. The resin was applied to the column and washed with two column volumes 50mM Na_2HPO_4, 300mM NaCl, pH 7 (Buffer B). The protein was eluted with Buffer B with 1M imidazole in increasing concentration from 0% to 100% over 6 column volumes in 1mL fractions using the AKTA FPLC system (GE Healthcare). Fractions containing protein were concentrated and further purified using Superdex 200 10/300 GL SEC column (GE Healthcare) and eluted with Buffer B using the AKTA FPLC system. SDS-PAGE gels showed loss of protein yield and no improvement in purity, thus an insoluble protein purification method via inclusion bodies was considered.

2.3 EXPRESSION AND PURIFICATION OF PHB1 IN INCLUSION BODIES

The following protocol was used for the (PHB1)-T3 construct as this protocol was adapted from a previous protocol used with this construct. This construct contains residues 52-197 of PHB1 in the pET46 vector with an enterokinase-cleavable N-terminal His_6-tag. Protein expression was done using the same method as seen in section 2.2 except main culture and

induction were done at 37ºC. Homogenized cells were stored and frozen in a buffer containing 50mM HEPES, 300mM NaCl, pH 7.5 (Buffer C). Following lysis via sonication, DNAseI and a working concentration of 6mM magnesium sulfate hexahydrate ($MgSO_4 \cdot 6H_2O$) was added and incubated at room temperature for 30mins. The insoluble material was collected using centrifugation at 5000xg for 20min at 4°C. The supernatant was discarded and the pellet was re-suspended via sonication in Buffer C with 0.1% dodecyl maltoside (DDM) and 10mM EDTA. The suspension was incubated on ice for 30 mins. The insoluble material was collected by centrifugation at 5000xg for 20min at 4°C. The pellet was re-suspended and sonicated into Buffer C with another step of centrifugation as earlier. The remaining pellet was re-suspended in 50mM HEPES, 300mM NaCl, 6M Urea, pH 8.0 (Buffer D) and was gently rocked overnight at 4°C. On the following day, any remaining undesired insoluble material was collected via centrifugation at 75000xg at 10°C. The supernatant was added to HisPur™ Cobalt Resin pre-equilibrated with two column volumes of Buffer D. Protein was eluted using batch method with 50mM HEPES, 300mM NaCl, 6M Urea, pH 7.5 (Buffer E) with increasing concentrations of imidazole. Batch fractions were collected and concentrated. The concentrate was then slowly dialyzed into 50mM HEPES, 2mM TCEP, pH 7.5 (Buffer F) with decreasing concentrations of urea at 4°C overnight with each buffer exchange with the final buffer condition of Buffer F with no urea content. This protocol was later applied to the final preferred construct, (PHB1)-25-252-$CHis_6$.

2.4 WESTERN BLOT FOR PROTEIN DETECTION

The presence of PHB1 protein following purification was detected using Western blotting. SDS-PAGE gels were loaded and run using the same conditions as for coomassie staining. The sandwich components were soaked in a buffer of 48mM Tris, 39mM glycine, 20% methanol, and 0.037% SDS at pH 8.3. From cathode to anode, the nitrocellulose membrane was placed on top of the filter paper stack, to which the gel was placed on top, and followed by another stack of filter paper completing the sandwich. Proteins from the polyacrylamide gel were transferred onto a nitrocellulose membrane using semi-dry electroblotting at 25V, 1.0A for 30mins. The membrane was transferred to the iBind Western System (ThermoFisher, USA). Blocking, binding of the HRP conjugated anti-His_6 antibody (Qiagen), and membrane washing was done using the iBind Western System commercial protocol. Following the blotting step, the membrane was incubated in Luminata™ Forte Western HRP Substrate (EMD Millipore, USA) for one minute at room temperature and imaged using a fluorescent detector.

2.5 CYSTEINE REDUCTION EXPERIMENTS

Aliquots of 0.5mg/mL (PHB1)-T3 were made. To the aliquots various amounts of 1M dithiothreitol (DTT) in Buffer C (see section 2.3) were added to generate various working concentrations ranging from 1-10mM in Buffer C. The mixtures were allowed to gently rock at 4°C overnight and loaded onto a 13% SDS-PAGE gel to observe the results.

2.6 CIRCULAR DICHROISM (CD)

(PHB1)-25-252-CHis$_6$ was diluted to a concentration of 0.204mg/mL using CD buffer containing 12.5mM Na_2PO_4, 200mM NaF, pH 7.0. CD spectra were collected using Circular Dichroism Spectroscopy with a Jasco J-810 Spectropolarimeter (Jasco Inc., Easton, MD, USA). Spectra were recorded in CD buffer between 260 nm and 190 nm, with a 1 mm cuvette and a 4 s integration time. Sample and buffer were measured in triplicate and after averaging the buffer was subtracted from the sample. The secondary structure content of the protein was determined from the experimental data using the DichroWeb analysis package and the CDSSTR algorithm. [39] Results were compared to theoretical predictions from GORIV. [40]

2.7 DYNAMIC LIGHT SCATTERING (DLS)

Data was collected using the Nano-S Dynamic Light Scattering system (Malvern Instruments Ltd., Malvern, UK) equipped with a 633nm laser and using a 173° scattering angle. All solutions were centrifuged at 13000rpm for 5 mins at room temperature to sediment any aggregates. Samples were also allowed to equilibrate to 20°C for 5min inside the DLS instrument. Each concentration was measured a total of five times and were also averaged for data analysis purposes. (PHB1)-25-252-CHis$_6$ samples were measured in a 45 µL quartz cuvette at a range of concentrations between 1-60 mg/mL. Two series of measurements were conduction with the first in Buffer F (see section 2.3) and the second with Buffer F with 300 mM NaCl. The highest protein concentration was measured first. Following concentrations were made by diluting the previous sample with the corresponding buffer. This was done to minimize the amount protein used.

2.8 ANALYTICAL ULTRACENTRIFUGATION (AUC)

Data was collected using the ProteomeLab™ XL-A Protein Characterization System (Beckman-Coulter, Canada) and the An-50 Ti 8-place rotor. Prior to performing the experiments, (PHB1)-25-252-$CHis_6$ samples were dialyzed into the desired buffer conditions (Buffer F or Buffer F with 300mM NaCl) overnight at 4°C. Reference solutions used were taken from the post-dialysis buffer of the samples to avoid differences in buffer content from the sample and the reference. Protein, (PHB1)-25-252-$CHis_6$, was tested at various concentrations ranging between 2-20mg/mL and in two different buffer conditions, Buffer F and Buffer F with 300 mM NaCl. Single cycle wavelength scans were conducted to determine the wavelength that will be used for the experiment. Experiments involving Buffer F were conducted at 309 nm, 18000 rpm with 120 scans at 15 min per scan. Buffer F with salt experiments were conducted at 305 nm instead with the same number and time of scans. Protein and buffer properties relevant for sedimentation analysis was determined using SednTrp and data analysis was performed with SedFit. [41, 42, 43]

2.9 SMALL ANGLE X-RAY SCATTERING (SAXS)

Experiments were performed with a Rigaku 3-pinhole camera on a gold-particle calibrated 200mm multi-wire 2D detector (NIST, Standard Reference Material 8012, USA). The instrument is equipped with a Rigaku MicroMax+200 microfocus sealed tube and Confocal Max-Flux (CMF) optics. The sample was illuminated with Cu-Kα radiation at 1.54Å. Buffer F and (PHB1)-25-252-$CHis_6$ at various concentrations (10, 20, 30, 40 mg/mL) were exposed for 2 to 4 hours and the raw data was processed with SAXGUI data processing software (Rigaku, USA). Data sets were merged and the ScÅtter and Primus programs were used to calculate the

radius of gyration (R_g) and the maximum particle dimension (D_{max}). [44, 45] These two parameters were used to perform ab initio modelling with low resolution structures generated with the DAMMIF program. [46] DAMAVER was used to average the models generated. [47]

2.10 TRANSMISSION ELECTRON MICROSCOPY (TEM)

Microscopy was performed at the National Microbiology Laboratory in Winnipeg, Manitoba, Canada using the FEI Tecnai F20 microscope with the help of Daniel Beniac and Dr. Timothy Booth. (PHB1)-25-252-$CHis_6$ samples of various concentrations ranging from 0.6-0.006 mg/mL under low salt (22 mM NaCl) and high salt (300 mM NaCl) conditions were adsorbed onto a formvar support film on 400-mesh copper grids. Adsorbed proteins were negatively stained with methylamine tungstate and were allow to air dry before being placed into the microscope. Images were taken at 80000x to 100000x magnification for each protein concentration sampled.

2.11 CRYSTALLIZATION ATTEMPTS

Protein crystallization screens: Crystal Screen 1 and Crystal Screen 2, Natrix 1 and 2 (Hampton Research), JBScreen Classics 1-8 (Jena Bioscience), Cation suite and $AmSO_4$ suite (Qiagen), and JCSG-Plus (Molecular Dimensions) were used to screen possible crystallization conditions. The initial crystallization trials were set up at protein concentrations of 5, 9, and 12 mg/mL. Drops were setup taking 0.4µL (PHB1)-25-252-$CHis_6$ protein and 0.6µL reservoir solution (crystallization solution). Sitting drop screens were made using the Gryphon-LCP (Art

Robbins Instruments, CA, USA) and set on 96-3LVR Intelli-Plates (Hampton Research, CA, USA). Based upon the results from the DLS and AUC experiments, another set of screens were repeated with the Hampton Research Crystal Screens 1 and 2 using 1 µL of 20, 40, and 60 mg/mL protein and 1 µL reservoir drops. Crystals were screened using a Rigaku MicroMax™-007 HF diffractometer.

3.0 RESULTS

3.1 PHB1 CONSTRUCTS

To check that PCR products of the correct sizes were produced, the products were loaded onto a 1.5% agarose gels. Annealing temperatures of 62 and 67ºC were tested. For inserts (PHB1)-31-252 and 28-252, an annealing temperature of 62°C produced the most product (Figure 5A, left) whereas a lower annealing temperature of 56°C was optimal for insert (PHB1)-22-252 (Figure 5A, right). Expected bands of 700bp were observed, indicative of correct PCR product sizes. Following ligation and cloning, a number of clones were picked and plasmid stocks were made. The plasmids were redigested with NdeI and XhoI to check for the presence of insert. The clones selected showed a high molecular weight fragment at approximately 5 kbp and a smaller fragment at 700 bp corresponding to the vector and insert, respectively (Figure 5C). Sequencing results confirmed that the clones contained the correct construct sequence corresponding to the residues of each insert followed by a C-terminal His_6-tag.

A)

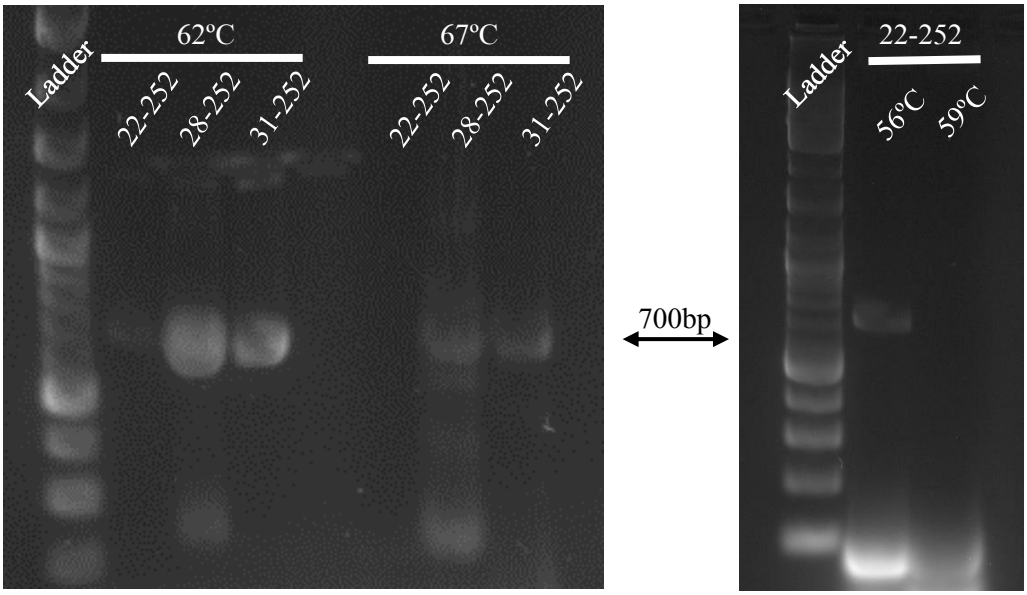

B)

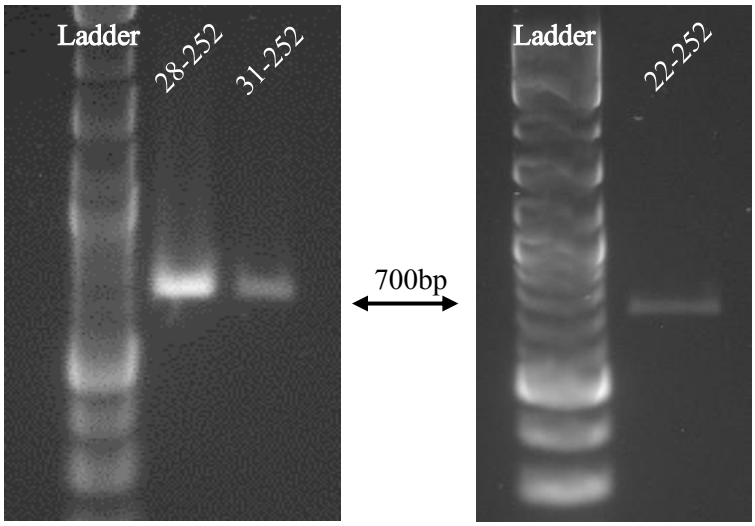

C)

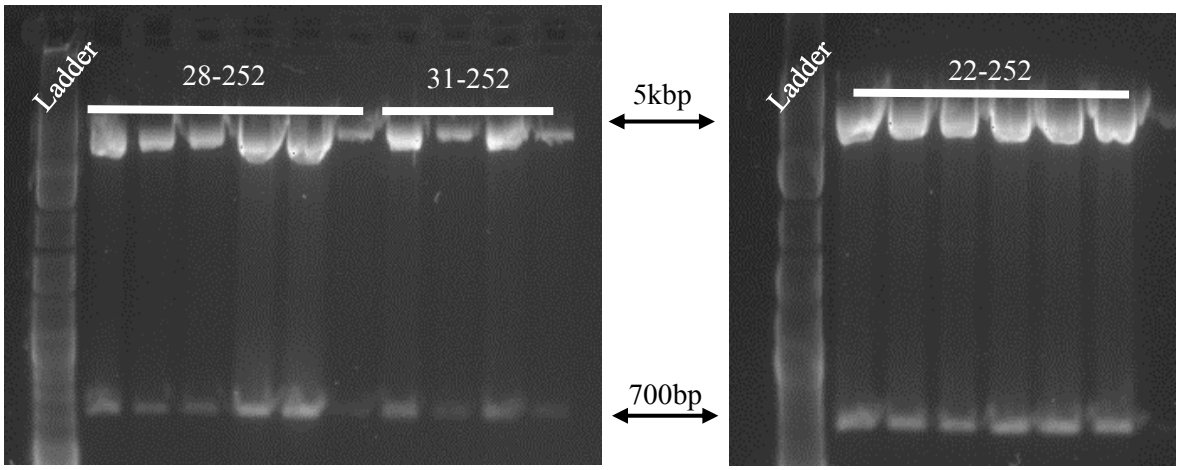

Figure 5: 1.5% agarose gels to observe products of PCR, restriction digest and cloning for PHB1 constructs. A, previous page) PCR products for PHB1 31, 28 (left), and 22 to 252 (right) at varying annealing temperatures. B) Products from NdeI/XhoI restriction digestion for 31, 28 (left), and 22 to 252 (right). C) Following insert ligation into vector pET21(a) and DH5α cloning, restriction digestion was used to confirm successful gene insertion for 31, 28 (left), and 22 to 252 (right).

The (PHB1)-25-252-CHis$_6$ construct was synthesized from a commercially purchased insert instead of performing PCR to bypass PCR reaction and save time. Sequencing results confirmed the plasmid contained a sequence corresponding to PHB1 residues 25-252 followed by a C-terminal His$_6$-tag.

(PHB2)-36-299-CHis$_6$ plasmid construction (Figure 6) showed similar results to the (PHB1)-31(and 28)-252-CHis$_6$ constructs. The PCR products from the 67ºC annealing temperature reaction were used for subsequent cloning. The PHB2-36-299 insert was approximately 800bp in size, which was observed on the agarose gel. Although construction was successful, the focus will be on the PHB1 constructs shown earlier.

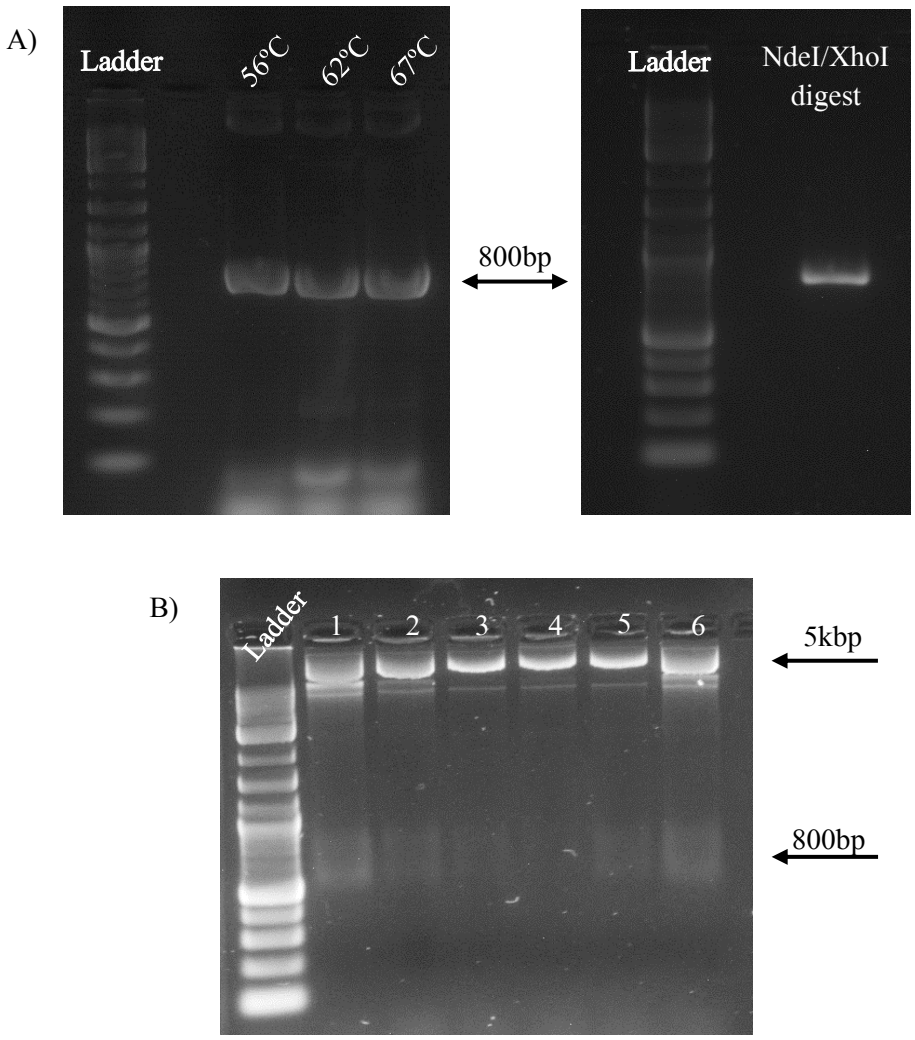

Figure 6: 1.5% agarose gels to observe products of PCR reactions, restriction digests and cloning for (PHB2)-36-299-CHis$_6$. A) PCR products for (PHB2)-36-299 (left) at varying annealing temperatures and restriction digest using NdeI and XhoI. B) Following insert ligation into vector pET21(a) and DH5α cloning, restriction digestion was used to confirm successful gene insertion.

3.2 PROTEIN EXPRESSION

3.2.1 SOLUBLE PROTEIN EXPRESSION

Production of soluble (PHB1)-31-252-CHis$_6$ was the first goal of the project. Protein was observed in the supernatant after cell lysis which suggested that isolating soluble protein was a possibility. It was clearly observed that the amount of soluble protein increased when the expression temperature was decreased from 30ºC to 20ºC. Surprisingly, despite the presence of an affinity tag, affinity chromatography did not sufficiently purify the protein. From the A280 traces, elution fractions showed large amounts of protein (Figure 7B). Western blot analysis was conducted to confirm the presence of the desired protein. Since fluorescent signals were observed, (PHB1)-31-252-CHis$_6$ was eluted but in low amounts (Figure 8). After concentration, the sample was loaded on to a size exclusion column for further purification. The SDS-PAGE indicated protein was present but after performing a Western blot, no PHB1 was present in the fractions collected (Figure 9).

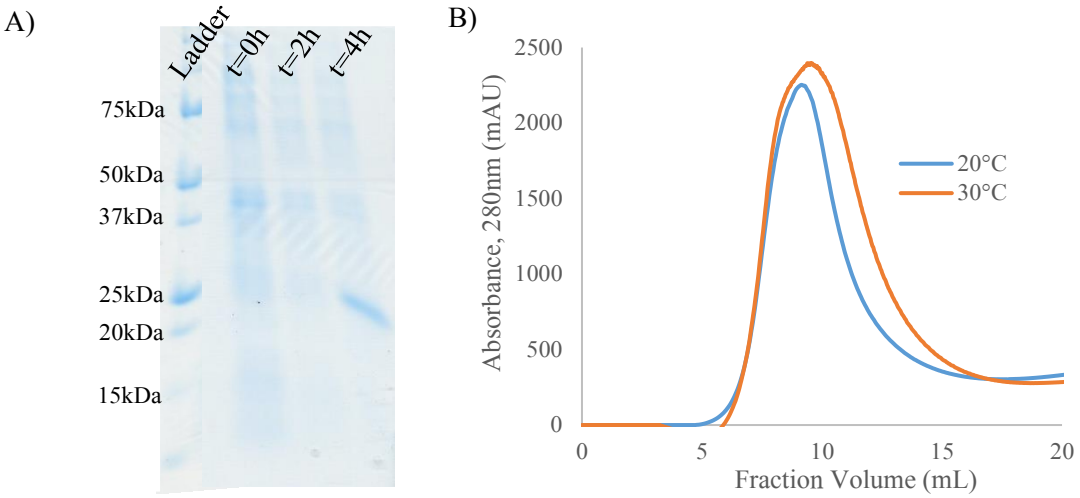

Figure 7: Results of soluble (PHB1)-31-252-CHis$_6$ production and nickel affinity chromatography. A) 13% SDS-PAGE gel depicting protein expression during induction after 0, 2, and 4 hours at 30ºC. B) Elution chromatogram from FPLC purification from 20°C and 30ºC. Absorbance was at 280nm.

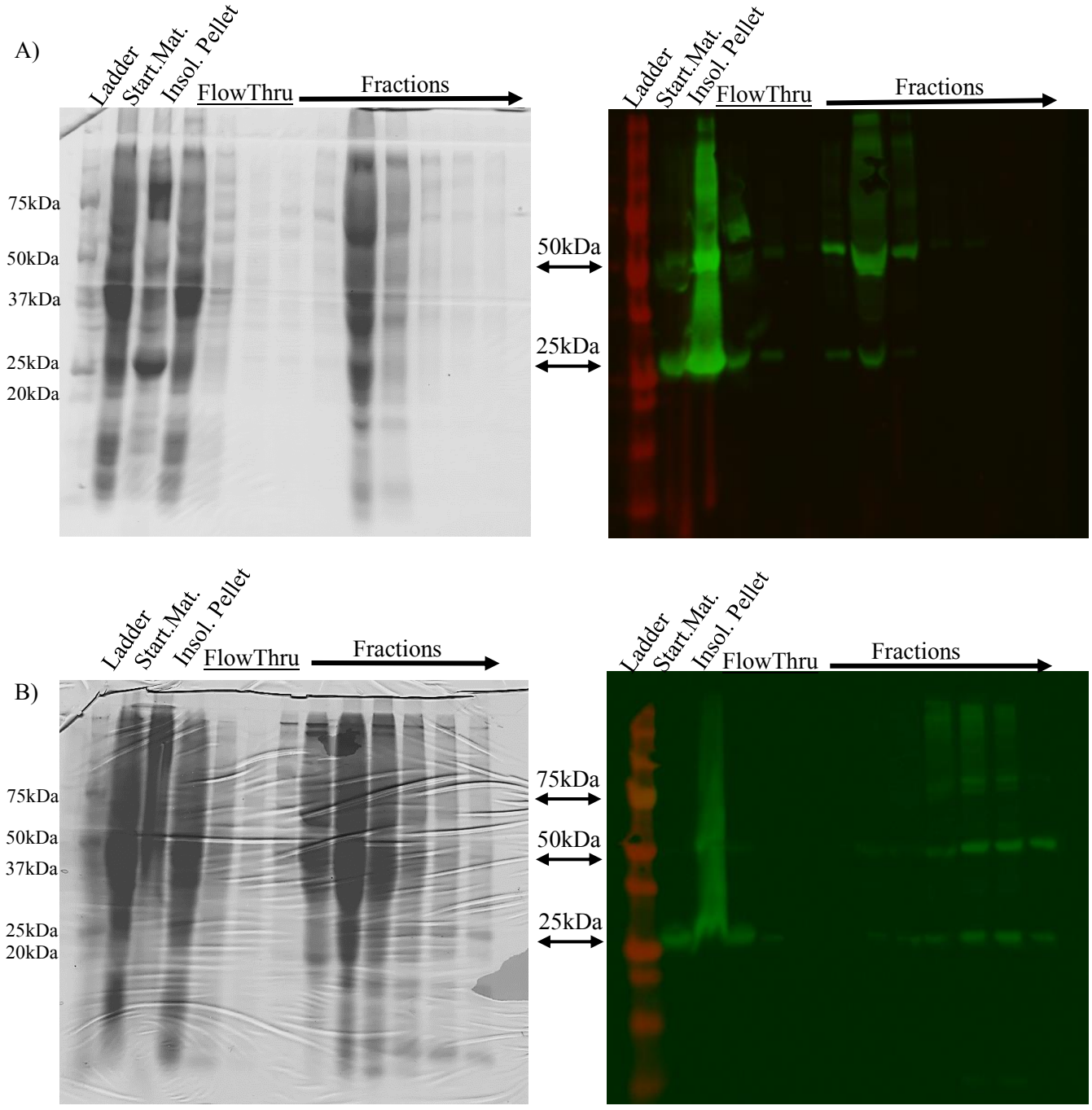

Figure 8: 13% SDS-PAGE gels (CBB dye) and corresponding Western blots of nickel affinity chromatography for soluble (PHB)-31-252-CHis_6 elution. A) Results of chromatography for 30ºC expression. B) Results of chromatography for 20ºC expression.

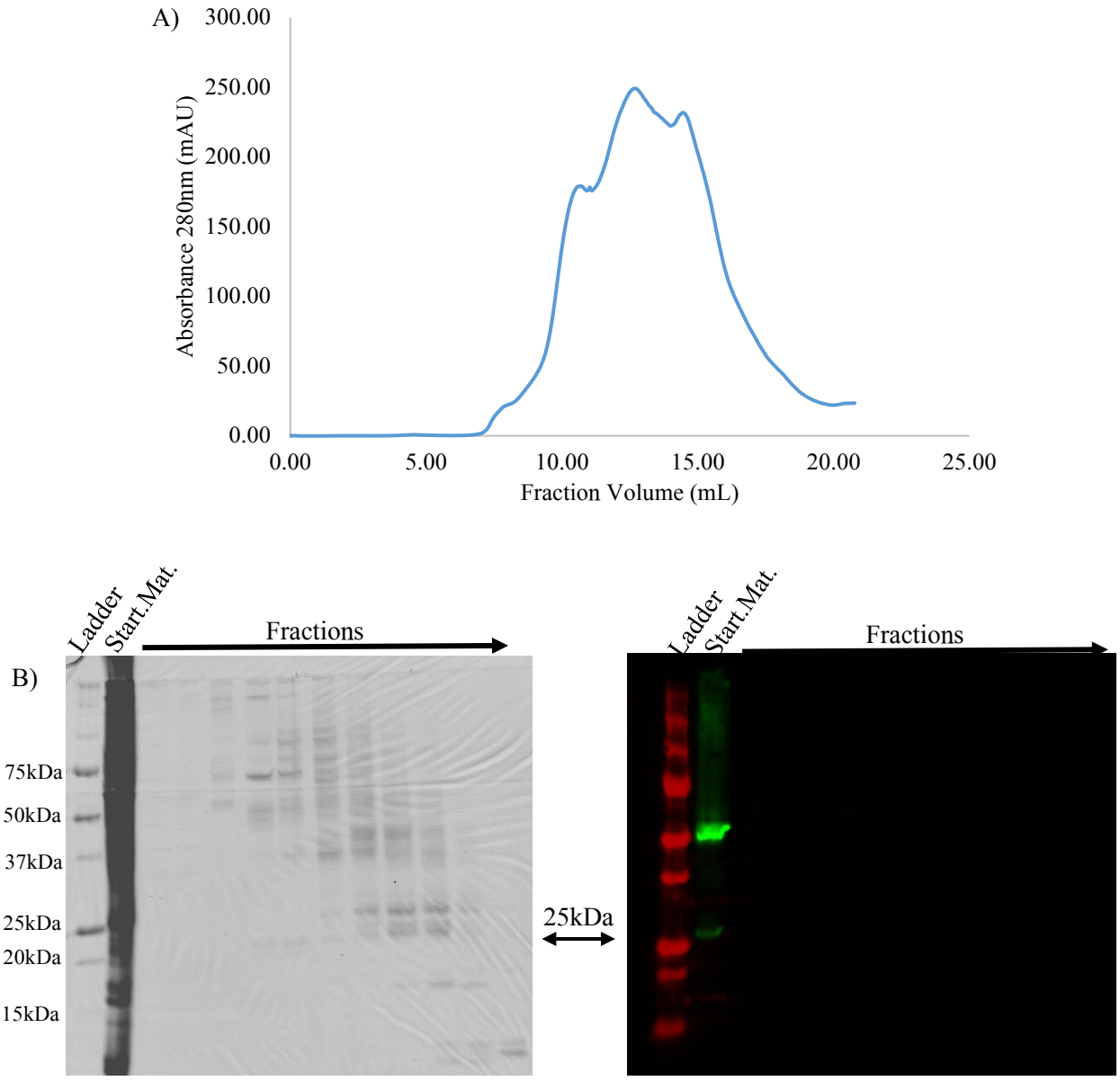

Figure 9: Results of size exclusion chromatography on Sdx200 column for (PHB1)-31-252-CHis$_6$. A) Elution chromatogram from FPLC purification. B) 13% SDS-PAGE gel image (left) with Western duplicate (right) of protein produced from cells grown at 20ºC.

3.2.2 INSOLUBLE PROTEIN PRODUCTION AND CYSTEINE REDUCTION

The results of initial experimentation showed that cell cultures grown at higher temperatures produced a larger amount of soluble PHB1. Therefore, a protocol was developed involving inducing insoluble protein production, following chemically denaturing the protein for purification, and then refolding the product. Initial attempts at purifying insoluble protein were with the (PHB1)-T3 construct. Insoluble protein was isolated from the cellular debris pellet formed following cell lysis. Starting material prior to affinity chromatography, when loaded onto the SDS-PAGE as a reference, showed very minimal undesired products as compared to that of initial soluble protein experiments (Figure 10A). Following affinity chromatography, the resulting batch fractions contained only desired protein thus no further purification was required. Gels showed a large proportion of protein with molecular weight similar to that of dimeric PHB. Reactions performed using DTT (not with TCEP for cost-effectiveness) decreased the amount of dimeric protein but not completely (Figure 10B). TCEP was used in later experiments.

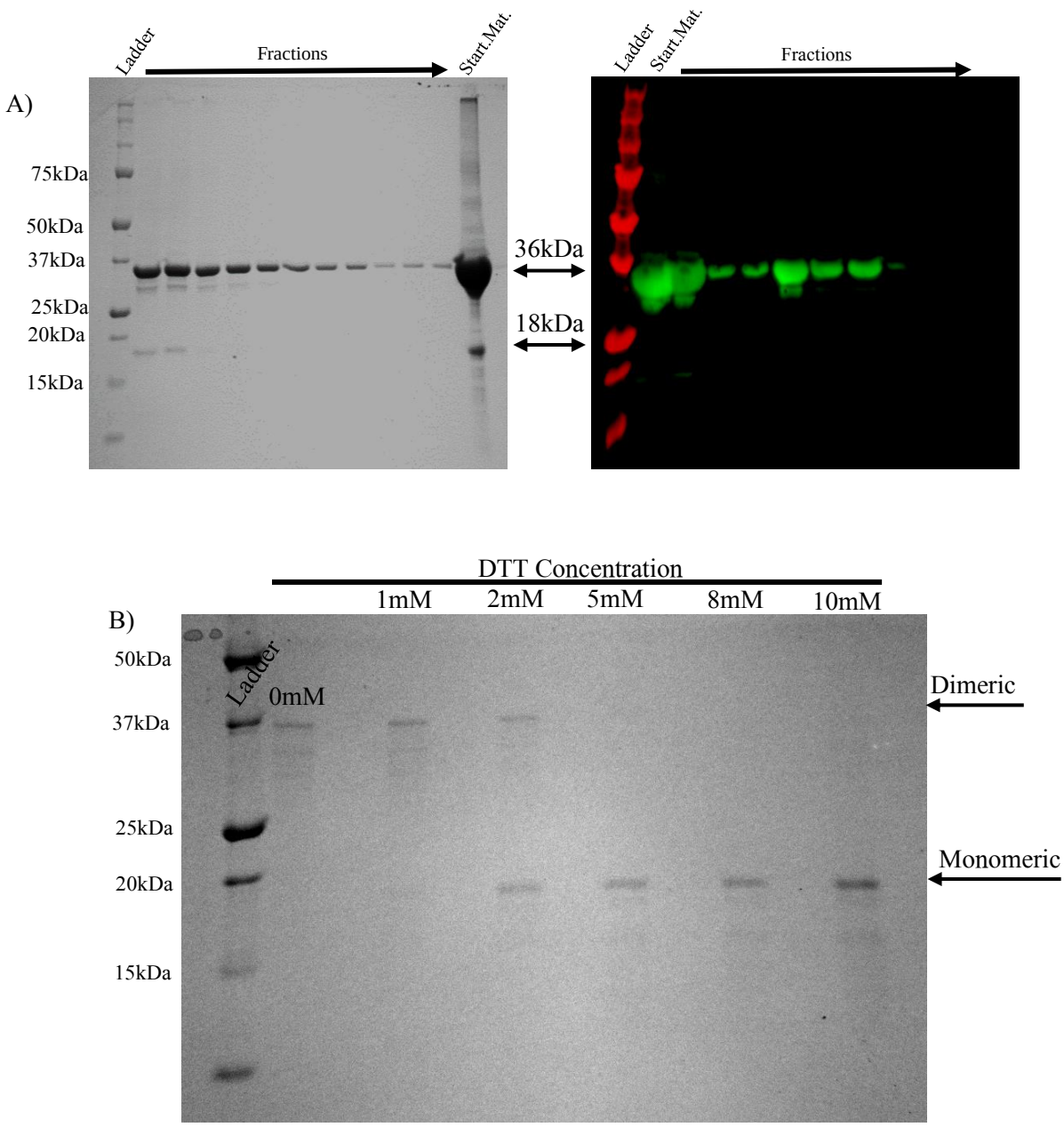

Figure 10: Results of batch nickel affinity chromatography for (PHB1)-T3 inclusion bodies. A) 13% SDS-PAGE gel of batch elution (left) with anti-His_6 Western blot duplicate (right). B) 13% SDS-PAGE gel image showing effect of increasing concentration of buffer DTT on the appearance of protein monomer

Dialysis was used to remove the denaturant and refold the protein. Initial attempts at refolding using Buffer C (with 2mM TCEP) resulted in protein precipitation. Lower salt buffers seemed to improve the refolding process thus the final buffer is Buffer F which contains 22mM NaCl. This protocol was later utilized for construct (PHB1)-31-252-CHis$_6$ with comparable purification success (Figure 11A). However, the protein proceeded to precipitate following refolding steps. (PHB1)-25-252-CHis$_6$ (Figure 11B) was developed and was observed to be stable during and after refolding. The following biophysical and structural experiments will involve only the new construct.

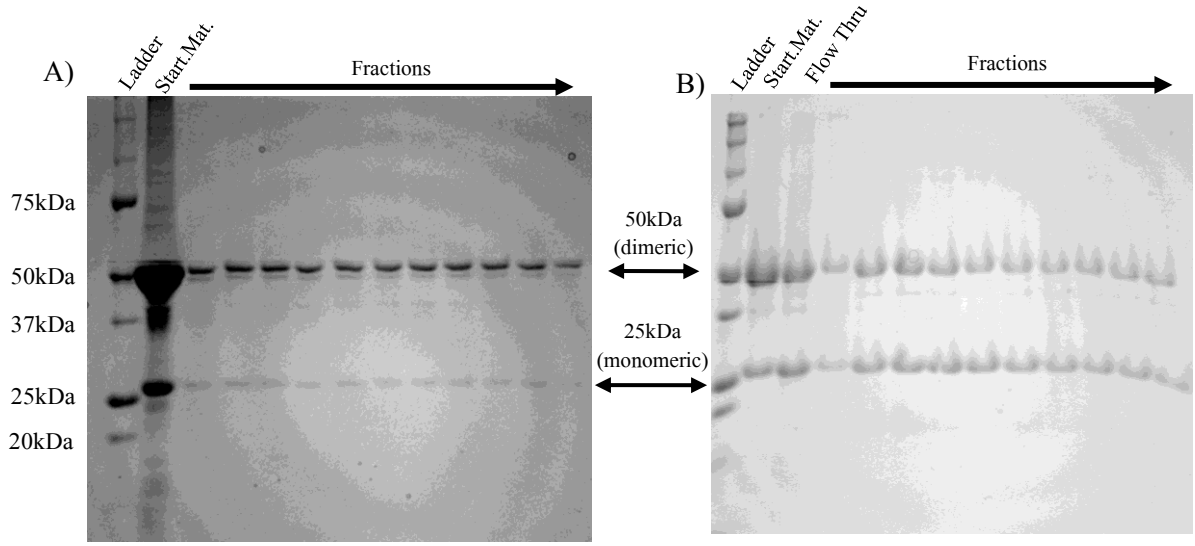

Figure 11: Results of batch cobalt affinity chromatography for protein purified from inclusion bodies. A) 13% SDS-PAGE gel of (PHB1)-31-252-CHis$_6$ purification. B) 13% SDS-PAGE gel of (PHB1)-25-252-CHis$_6$ purification.

3.2.3 CIRCULAR DICHROISM SPECTROPOLARIMETRY

The following plot is the CD plot of (PHB1)-25-252-CHis$_6$ (Figure 12). The first conclusion that can be made from the spectrum is that the protein does have some secondary structure. The spectrum is not consistent with that of an unfolded protein. Further analysis using the DichroWeb server and the CDSSTR analysis programme with all usable sub-datasets indicated that the protein's secondary structure consists of approximately 16% α-helix, 28% β-sheet, 18% turns, and 36% random coil. This convolution agrees with the features of the spectrum. A clear local minimum at 208 nm is indicative of an α-helix. A broadened local minimum resembles a combination of the 222 nm α-helical and 218nm β-sheet negative peaks. GORIV predictions show disagreeing proportions as seen in Table 1. The predicted level of helix is significantly greater with the suggested proportion of helix being 53.6% and 8.9% sheet. Random coil predictions were similar, however, at 37.6%. Measurements taken below 190 nm were not used as high tension voltage exceeded acceptable values.

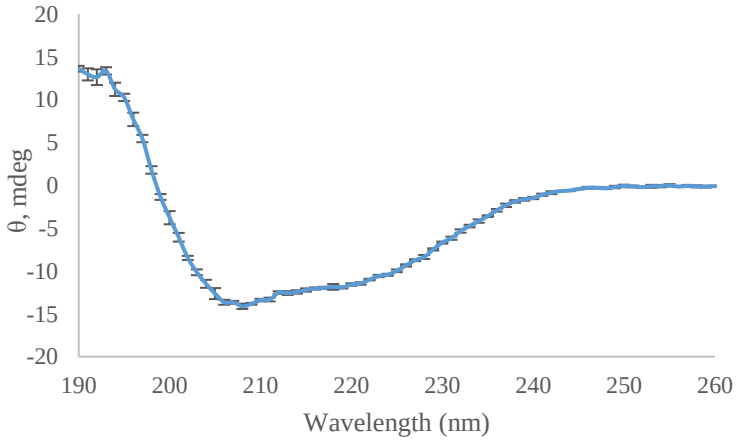

Figure 12: Results of CD experiment for (PHB1)-25-252-CHis$_6$. Local minimum at 208 nm and a broadened 222 nm peak suggest a folded protein with both alpha helical and beta sheet structure.

Prediction	**α-helix**	**B-strand**	**Turns**	**Random Coil**	**Total**
GORIV	0.536	0.089	--	0.376	1.00
DichroWeb	0.18	0.3	0.13	0.38	0.99

Table 1: List of predictions of (PHB1)-25-252-CHis$_6$ secondary structure composition. Values based on known amino acid sequence (GORIV) or numerical data of CD experiment (DichroWeb).

3.3 STRUCTURAL AND BIOPHYSICAL CHARACTERIZATION

3.3.1 DLS

The DLS experiments were conducted in order to determine the mono-dispersity and homogeneity of the protein product by its hydrodynamic radius. A total of five trials were performed for each concentration and later averaged for data analysis. Data showed that (PHB1)-25-252-CHis_6 was generally mono-dispersed by percent volume (%Vol). By intensity (not shown), larger species were observed but the population was low enough that under %Vol the amount was negligible. The protein hydrodynamic radii were compared among the various concentrations tested, 1-61mg/mL for high salt (300mM NaCl) and 1-57mg/mL for low salt (22mM NaCl). A trend of increasing size with decreasing protein concentration was observed. Under both high salt and low salt conditions, this was observed with the high salt buffer showing a less drastic change in size. In a buffer containing 300mM NaCl, the hydrodynamic radius ranged from 11-15nm whereas in 22mM NaCl, the range was from 5-15nm.

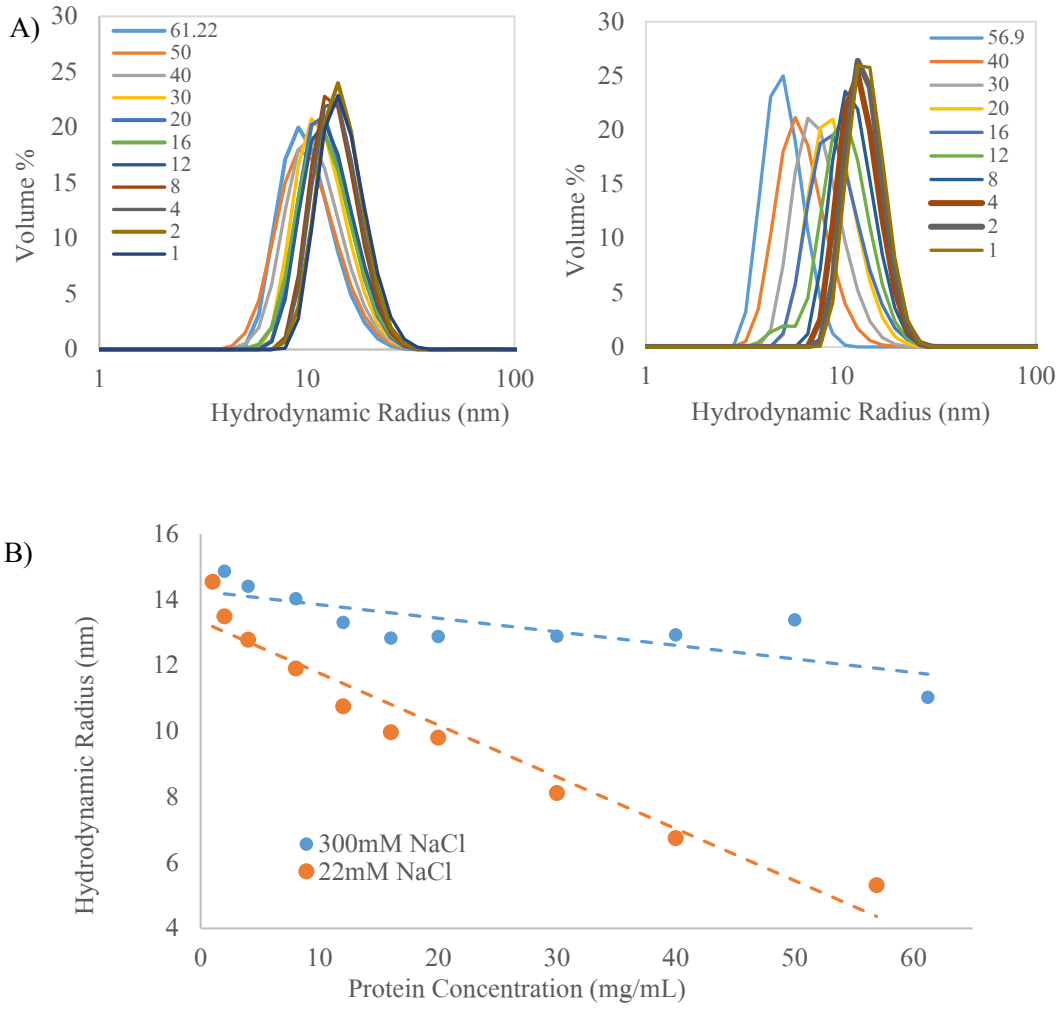

Figure 13: Results of DLS experiments for (PHB1)-25-252-CHis$_6$. A) DLS spectra for (PHB1)-25-252-CHis$_6$ under two NaCl concentrations, 300mM (left) and 22mM (right). B) Plot correlating peak radii from the spectra and protein concentration illustrating decrease in hydrodynamic radius with increasing protein concentration.

3.3.2 AUC

AUC experiments were also used to determine the mono-dispersity and homogeneity of the (PHB1)-25-252-CHis$_6$ sample but by analysing protein size in terms of sedimentation rate in Svedberg units. Experiments were conducted with protein concentrations ranging from 2-20mg/mL and under two different salt concentrations, low (22mM NaCl) and high (300mM). Similar to observations made from the DLS experiments, protein at higher concentrations adopt a smaller sized oligomer whereas at lower concentrations higher order oligomers were observed. Higher salt condition allowed the protein to adopt larger particle sizes than that of the lower salt condition. In a 22mM NaCl buffer condition, the protein's sedimentation rate ranged from approximately 9-15 Svedberg units and in 300 mM NaCl buffer the range is from 13-22 Svedberg units. Intensities of each peak decreased with decreasing protein concentration.

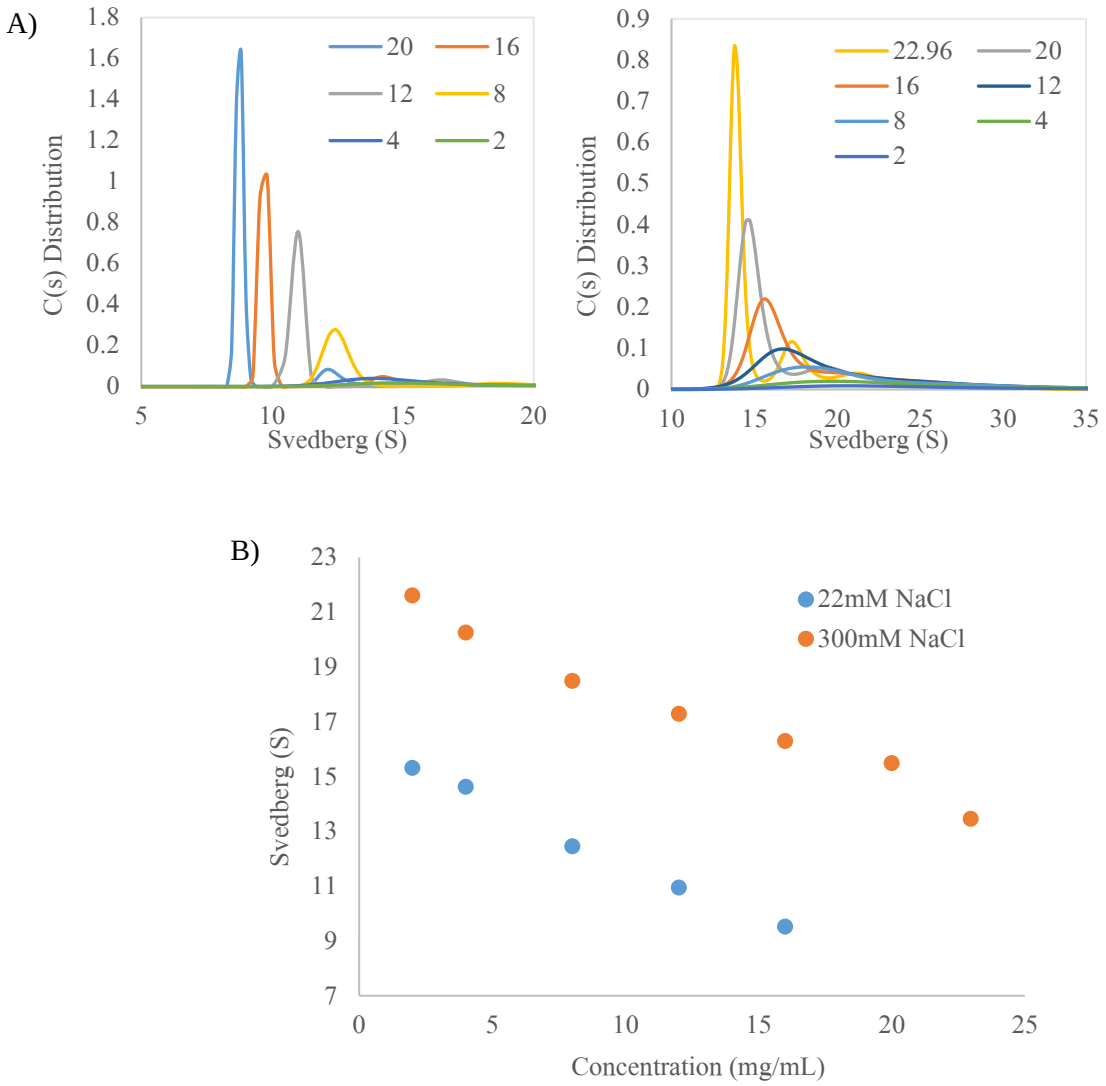

Figure 14: Results of AUC experiments for (PHB1)-25-252-CHis$_6$. A) AUC spectra for (PHB1)-25-252-CHis$_6$ under two NaCl concentrations, 22mM (left) and 300mM (right). B) Plot correlating peak radii from the spectra and protein concentration illustrating decrease in hydrodynamic radius with increasing protein concentration.

3.3.3 SAXS

SAXS experiments were conducted with (PHB1)-25-252-CHis$_6$ concentrations of 10, 20, 30, and 40mg/mL. Below is a table listing the calculated R_g and D_{max} as well as the Kratky and P(r) distribution plots, made using ScÅtter and Primus. The DAMMIF structures (examples shown below) were averaged with DAMAVER to generate the structure below.

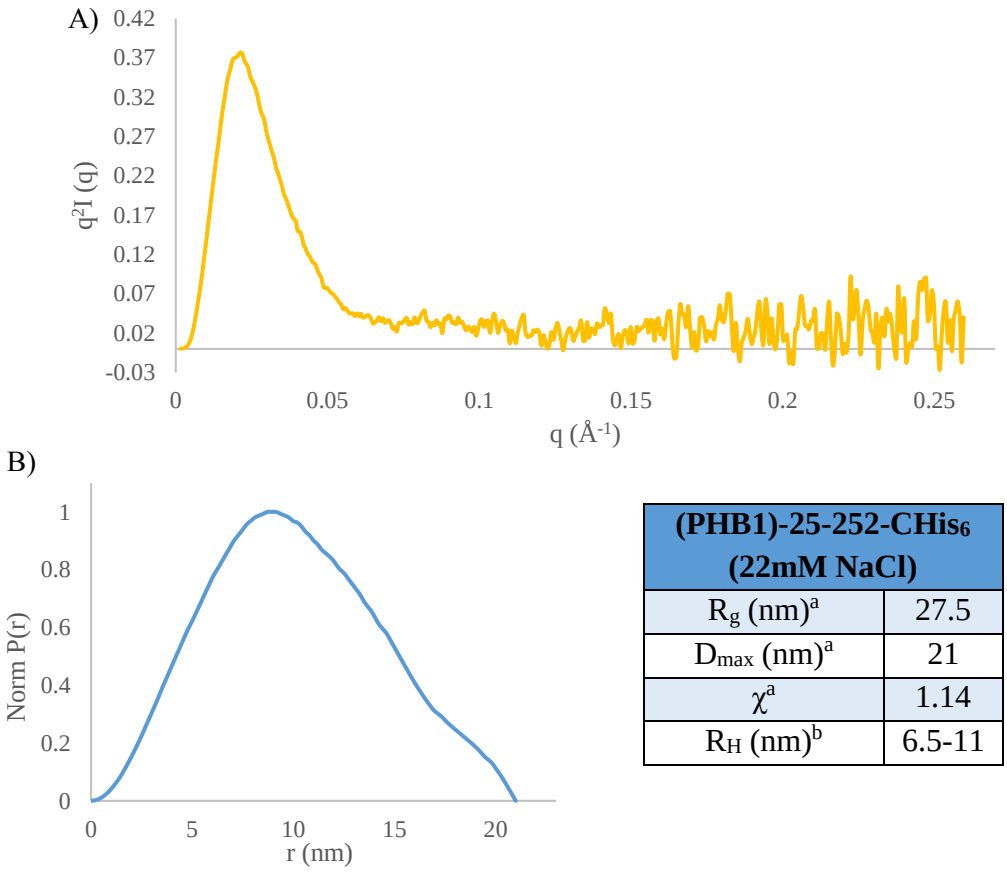

(PHB1)-25-252-CHis$_6$ (22mM NaCl)	
R_g (nm)[a]	27.5
D_{max} (nm)[a]	21
χ[a]	1.14
R_H (nm)[b]	6.5-11

Figure 15: SAXS results and plots for (PHB1)-25-252-CHis$_6$. A) Kratky plot and B) Pair-distance distribution plot with D_{max} set as 21nm.

Table 2, above right: List of structural properties determined during SAXS analysis. R_g is the radius of gyration, D_{max} is the maximum particle diameter, and χ is the goodness of fit of data to the parameter set. a = derived from SAXS, b = derived from DLS.

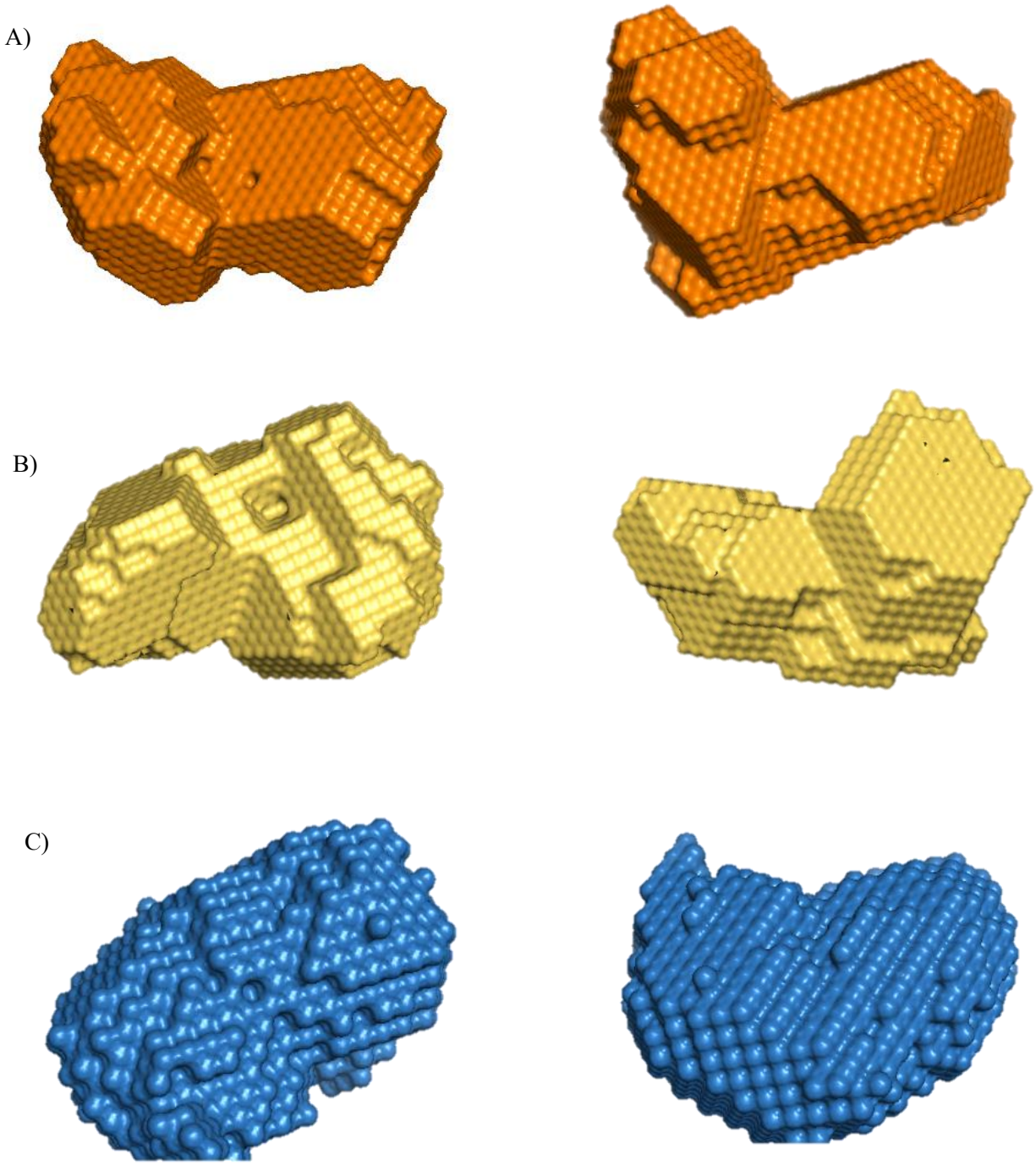

Figure 16: (PHB1)-25-252-CHis$_6$ DAMMIF structure models based on interpreted SAXS data with A) top two (orange) and B) middle two (yellow) being individual predictions. C) The bottom structure (blue) represents the average of all predictions.

3.4 TRANSMISSION ELECTRON MICROSCOPY

DLS and AUC results clearly demonstrate that (PHB1)-25-252-CHis$_6$ adopts a very large oligomeric state in solution. This provided the possibility of visualizing the protein using electron microscopy. Several concentrations of (PHB1)-25-252-CHis$_6$ ranging from 0.6mg/mL to 0.006mg/mL were adsorbed onto the support grid and under high or low salt buffer conditions. At higher concentrations a “lawn” of particles were observed to adsorb onto the grid surface making it impossible to identify single particles. However, diluting the protein to 0.006mg/mL allowed for single particles to be distinguishable. This was true for both salt concentration conditions. From the images collected, two major shapes were observed, circular and elongated tubes. However, upon further inspection more circular particles were observed under higher salt conditions. The diameters of the circular particles ranged from 16-20 nm whereas the tubes had lengths up to 27.8 nm.

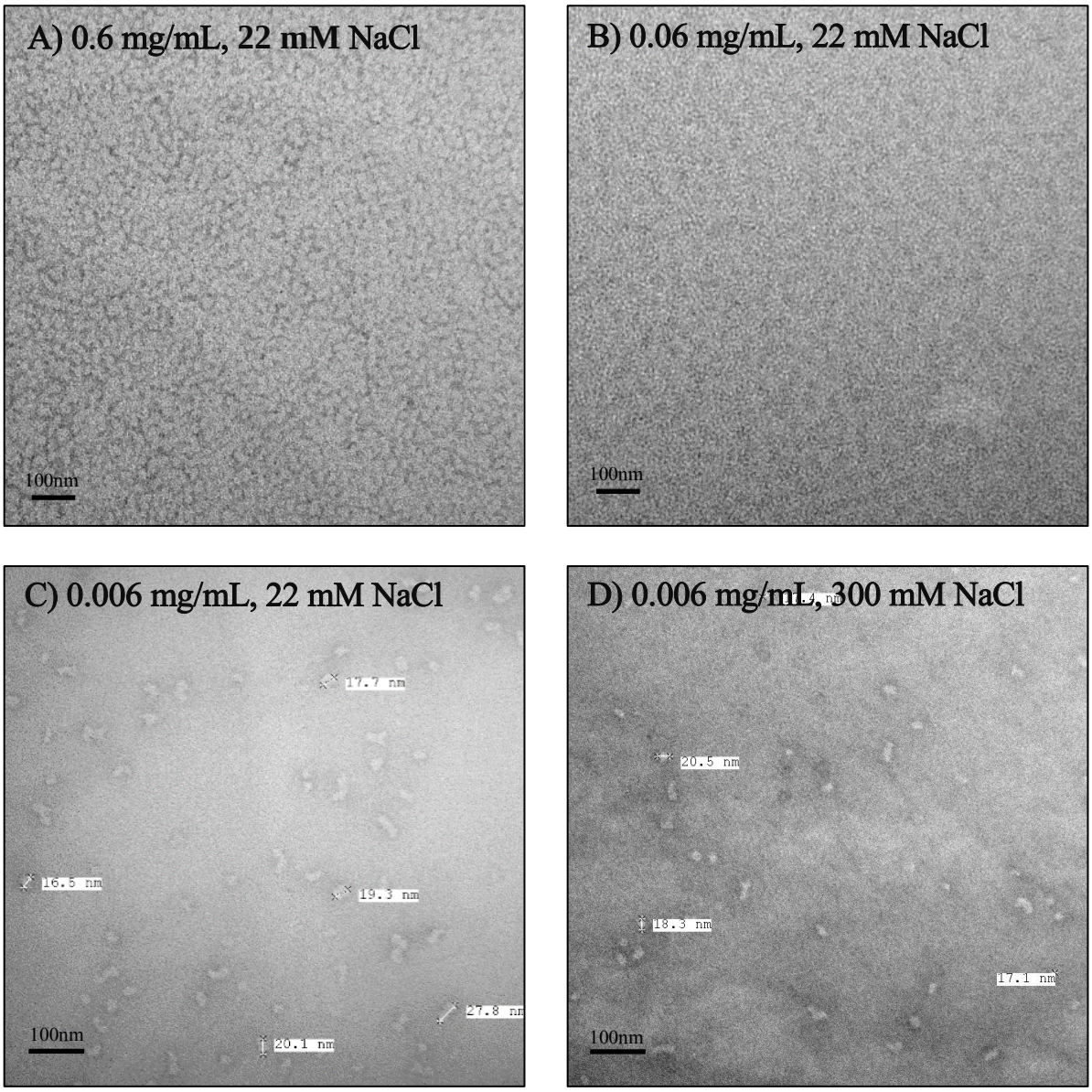

Figure 17: TEM micrographs of (PHB1)-25-252-CHis$_6$. Images were taken using the FEI Technai F20 microscope and methylamine tungstate as the stain. Higher concentrations of protein in Buffer F were adsorbed first at A) 0.6 mg/mL and B) 0.06 mg/mL. Lower protein concentrations of C) 0.006mg/mL showed distinguishable particles. D) Protein at 0.006mg/mL and in Buffer F with 300mM NaCl was also imaged.

3.5 CRYSTALLIZATION

At lower protein concentrations precipitation was observed in approximately 50% of the drops. However, a number of potential hits were observed for screens: JBS Classics, Cation Suite, and Natrix. Further X-ray analysis, using the diffractometer, revealed that all crystals were of salt. In light of the DLS and AUC results, the crystallization experiments were repeated with 20, 40, and 60 mg/mL protein concentrations. These crystallization trials were less successful as at a protein concentration above 40 mg/mL the protein became too viscous to properly setup the drops, whilst the 20 mg/mL trials contained significantly more precipitate than the initial concentration series.

4.0 DISCUSSION

The goal for this project was to produce high quality protein with the aim of crystallizing PHB1. Residues comprising the transmembrane domain were removed to avoid having to work with detergents whilst still keeping the PHB and coiled-coil domains intact for structural studies. The constructs were also designed with truncations made in between GORIV-predicted secondary structures to avoid truncating partial structures (Table 3). For example, PHB1-31-252-$CHis_6$ was designed to avoid truncations part-way through the helix predicted between residues 26-30. PHB1-22-252-$CHis_6$ was designed to include the sheet predicted to begin at Val22. The C-terminal truncation at Ser252 includes the coiled-coil domain of PHB1.

Amino Acid Sequence WT PHB1	11'- KFGLALAVAG GVVNSALYNV DAGHRAVIFD
GORIV Prediction	HHHHHHHHCC CEECCHHHHH CCCCHHHHHH

Table 3: Human PHB1 amino acid sequence (residues 11-40) aligned with GORIV secondary structure prediction. Illustrates predicted residue contribution to protein secondary structure and gene truncation strategy. GORIV legend: C – random coil, E – β-sheet, H – α-helix

Initial work involved expressing protein in the soluble fraction. Cell cultures were grown at varying temperatures and it was shown that lower temperatures increased the production of soluble protein. There are a number of factors that may have contributed to this occurrence. [48] Temperature affects the kinetic factor in protein aggregation. With increased temperature the propensity of aggregation increases as well. Studies conducted with other proteins such as human interferon α-2 and phosphoglycerate kinase report a decrease in protein aggregation at lower temperatures. [49, 50] At greater temperatures, water-water interactions begin to breakdown

allowing for hydrophobic interactions between protein residues to predominate. This increase in hydrophobic interactions and attraction results in increasing protein aggregation. [51] Although, PHB1 is a different protein, the explanation can be translated to PHB1. Additionally, at lower temperature there is a decrease in bacterial protease expression and optimal chaperone activity, thus, allowing recombinant protein to be produced with minimal degradation and with facilitated folding. [52] However, a sacrifice must be made owing to decreased cell growth and gene expression rates. [48] This was remediated by allowing for 16 hours (overnight) of induced expression time instead of the 4 hours used for higher temperature experiments. Following affinity chromatography, the SDS-PAGE gels (Figure 7B & C) showed very little improvement in isolating (PHB1)-31-252-CHis$_6$ as fraction lanes showed large amounts of eluted protein with molecular weights inconsistent with monomeric or multimeric PHB1-31-252-CHis$_6$. Since (PHB1)-31-252-CHis$_6$ contained a His$_6$-tag, a Western blot was performed to help interpret the results of the affinity chromatography. Fluorescent bands observed corresponded to only monomeric (25 kDa), dimeric (50 kDa), and some trimeric (75 kDa) (PHB1)-31-252-CHis$_6$, with no bands corresponding to the other proteins observed in the coomassie-stained gel. Therefore, this chromatography step resulted in elution of both desired and undesired protein. A possible reason for the presence of undesired protein may be due to PHB's ability to bind to various proteins. PHB is known to bind to many proteins in order to mediate cell signalling as discussed in the introduction. Since the soluble protein was isolated, it may have started non-specifically binding to other bacterial proteins. This interaction may have attributed to other proteins becoming bound to the resin via the affinity-tagged protein.

Concentrated protein was passed through a Superdex 200 column. Interestingly, following the column, peaks was observed in the UV absorbance spectrum but not very high in

intensity. The low intensity UV absorbance agreed with the low population of UV-absorbing residues including only Trp60. However, the SDS-PAGE indicated the presence of protein but corresponded to incorrect molecular weights. Western blots showed similar results as no His_6-tagged proteins were detected (Figure 9B). Therefore (PHB1)-31-252-$CHis_6$ may have bound to the size exclusion resin preventing it from eluting. Methods exists to remediate this problem such as inclusion of detergent or increase in ionic strength of the elution buffer to decrease hydrophobic interactions between the protein and column resin. [53] However, the lack of improved PHB isolation following affinity chromatography suggests a different method should be investigated. Previous work with PHB1 in the Suresh Mishra group encouraged utilizing the cell's way of forming inclusion bodies for protein production.

From earlier experimentation, PHB1 could be expressed in inclusion bodies when cells were cultured at higher temperatures. A method for purifying PHB1-T3, (PHB1)-31-252-$CHis_6$, and eventually (PHB1)-25-252-$CHis_6$ was developed from previous work from the Mishra Group. The newly developed method greatly improved protein purification as the inclusion bodies contributed to protein isolation prior to any chromatography as shown in the starting material lanes in Figures 10 and 11. However, affinity chromatography was still used to maximize PHB1-31-252-$CHis_6$ isolation. The protein was refolded via dialysis. Initially, the dialysis protocol involved using Buffer C and decreasing concentrations of urea. However, this caused significant protein precipitation. Thus various dialysis conditions were tested. Conditions tested included lower salt conditions with the most successful being Buffer F which contains no additional salt except for any NaCl that forms from pH adjustment titrations which equates to approximately 22mM NaCl. Very minimal precipitation occurred even when the sample was concentrated up to a concentration of approximately 60mg/mL. It would be interesting to observe

if there are any structural implications that come with refolding under lower salt conditions. Dynamic light scattering, analytical centrifugation, small angle X-ray scattering, and transmission electron microscopy were used to study these effects on the structure of (PHB1)-25-252-$CHis_6$ as well as to determine why the protein is stable under both salt conditions. While salts are known to have and effect on protein folding, the effect is not fully understood. [54] Though only speculation, the presence of salt may have prevented particular regions of PHB1-25-252-$CHis_6$ from interacting with one another, thus influencing the protein to adopt an unfavourable and unstable state.

Initial experimentation and protein expression were done with (PHB1)-31-252-$CHis_6$. As mentioned earlier, difficulties with protein stability were experienced with this construct (Table 3). Further GORIV secondary structure predictions showed a possible helix comprised of residues 26-30. This helix was included to make the construct that would be used for structural studies, (PHB1)-25-252-$CHis_6$. The addition of the extra residues improved protein stability as this new construct did not precipitate during and after refolding, unlike the previous construct.

Artificially refolding protein raises concerns of the protein being improperly folded. Since there are no previously known structures of PHB, CD spectroscopic predictions and deconvolutions were used to determine possible secondary structure features and proportions. The CD spectrum provides a qualitative determination whereas calculations with DichroWeb and GORIV predictions generate quantitative proportions of secondary structure features. The CDSSTR algorithm was the selected calculation method which utilizes a bank of reference proteins. In Figure 12, CD spectrum analysis and GORIV results suggest a predominantly helical protein. Interestingly, the DichroWeb calculations suggest otherwise. Due to this discrepancy, it is not possible to determine whether or not the protein is properly folded. At this time, no activity

assay was available that could be used to assess if PHB1-25-252-CHis$_6$ is properly folded. However, the spectrum shows no characteristics resembling an unfolded protein thus it can be concluded that the protein has adopted some secondary structure.

DLS results showed that (PHB1)-25-252-CHis$_6$ is homogenous. Despite the changes in hydrodynamic radius observed, the protein remains mono-dispersed over all concentrations surveyed. This meant that the protein may be suitable for crystallization and SAXS experiments. Further investigation led to interesting observations of the behaviour of (PHB1)-25-252-CHis$_6$ in solution. As concentration increases, the overall hydrodynamic radius decreases. This would be considered the opposite of what is expected with most proteins. Normally, as protein concentrations increase, aggregation occurs leading to larger particle sizes and hydrodynamic radii. It is possible that the intermolecular interactions between hydrophobic and hydrophilic residues may be involved. Hydrophobic residues interacting with other hydrophobic residues, and similarly with hydrophilic residues, are responsible for protein complexation. However, at greater concentrations in combination with the protein's propensity to form oligomers, the oligomerization may have become too excessive for these interactions to maintain it's size. This would cause the complex to collapse and form smaller particles.

The effect of salt on the hydrodynamic radius of (PHB1)-25-252-CHis$_6$ was also studied. The protein, under lower salt conditions, surveyed a larger hydrodynamic radius range than when in a high salt buffer condition. Although protein aggregation remains to be completely understood, it may be possible to explain this behaviour by considering the hydrophobic interactions between the protein and the buffer. At an optimal salt condition, the ions begin to electrostatically neutralize charged residues on a protein's surface. However, as salt concentrations increase above a certain threshold, the excessive surface charge causes individual

proteins to aggregate and neutralize the extra charges. Similarly, for proteins at low salt conditions, charged residues were not neutralized by buffer salts, protein aggregation occurs to neutralize the charges. [55] This would also explain the consistent sizes of (PHB1)-25-252-$CHis_6$ in the 300mM NaCl buffer at varying protein concentrations. The neutralized residues prevent (PHB1) -25-252-$CHis_6$ from extensively aggregating.

AUC results complemented the results of the DLS experiments. The AUC showed that (PHB1)-25-252-$CHis_6$ exists as a higher order oligomer at lower concentrations. Larger size range seen in the DLS for lower salt conditions, however, was not observed. The size distribution seems to be approximately the same for both salt conditions. It is also important to note that the intensity of each peak decreases as well as broadens out as the concentration decreases. A wavelength scan was performed into order to determine the wavelength to be used for the experiments. The wavelength selected must be absorbed readily by the protein sample. This allows for observing difference between the protein sample and the reference blanks. [35] Over the entire concentration range studied, the higher concentrations absorbed more readily at the experimental wavelengths but drastically dropped as the concentrations decreased. This may have affected the resolution of analysis for those concentrations but the position of the peaks still indicates large particles at the lower protein concentrations. As mentioned earlier, the DLS and AUC were used not only for biophysically characterizing (PHB1)-25-252-$CHis_6$ but also for determining the homogeneity of the protein sample required for SAXS experiments.

According to the DLS and AUC experiments, the (PHB1)-25-252-$CHis_6$ sample was predominately monodispersed. When analyzing the intensity percent distributions peaks pertaining to larger species, up to 100 nm in radius, were detected (not shown). However, according to the volume percent distribution, there is a very small amount of the larger species.

Unlike the volume percent distribution shown in Figure 13 which describes a protein's size based on the volume, intensity percent distribution quantifies the scattering intensity of each species within the sample. The scattering intensity increases for larger molecules. [32, 33, 34] This raised concerns with the SAXS data collection becoming affected by the small number of large particles but the SAXS experiment was followed through, regardless. The program, Primus (ATSAS, EMBL, Germany), was used to generate the Kratky plot. The plot indicates the protein was folded when compared to common Kratky plots with similar characteristic curves. [38, 56] Considering that the protein adopts a structure with a large hydrodynamic radius and adding the observation of a folded protein, the protein particle might be a complex composed of a large number of monomers. The P(r) distribution plots resembles those characteristic of globular protein but the presence of a shoulder at greater D_{max} may contribute to some multi-domain protein structure. [38, 56] The overly large particle size may play a factor in this discrepancy. The large and difficult to interpret oligomeric size of (PHB1)-25-252-CHis$_6$ prevents any reliable conclusions to be made from the DAMMIF structure predictions. However, a consistent model was observed. The structures depict a large globular structure with a bend or a kink towards the center. A ring-like structure was anticipated but may not be possible without a PHB2 homologue present.

The various structural experiments conducted clearly show that the protein forms very large complexes. Although it is unknown if the complex is ordered or not, the size encouraged pursuing electron microscopy for some preliminary structural information. A lawn of particles was observed for the higher concentrations of protein due to an excessive amount of protein being adsorbed onto the grid. Decreasing the protein concentration remediated the problem. Upon doing so and with further investigation, the protein adopted either a circular or an

elongated tube on the grid. When compared to the hydrodynamic radii calculated from the DLS experiments, the sizes observed in the microscope were not exact but similar. The theory regarding the capsule or vault-like structure of PHB1 compliments the two different orientations observed on the microscope. If the capsule were to be viewed from the two ends, the apparent shape would be circular, and elongated if viewed from the side; similar to the different faces of a tube or cylinder.

Protein crystallization proved to be very difficult and inconclusive. Crystals were observed in the various screens made, all of which had different morphologies. When analyzed with the diffractometer, only salt peaks were observed indicating that the crystals were made of salt. Higher protein concentration screens were also created. Since PHB1 was observed to adopt a very large complex in solution, the amount of protein per drop might not have been enough for forming sufficiently sized crystals. This, however, created another problem regarding the amount of protein and the behaviour of the sample. The sample was observed to be very viscous making it very difficult to form proper drops and for mixing. In addition, the large amount of protein led to high levels of precipitation preventing any crystallization from occurring. His-tags are flexible and are known to increase the propensity for protein aggregation. This may negatively affect how the purified (PHB1-25-252-CHis_6) crystallizes. [57] However, some protein structures have been solved with intact His_6-tags. [58, 59]

The construct used for the above experiments contained a non-cleavable affinity tag. The tag may be a factor in the above structural results. Future experiments will include developing a tag-free protein to prove the validity of the results shown. However, the electron microscopy images from Tatsuta showed formation of the PHB rings with a PHB construct with a histidine tag still attached. This result suggests the observations made from the above experiments may

still be valid. Tag-free protein will be considered, regardless, in hopes of improving structure determination.

5.0 FUTURE DIRECTIONS

Since a tag-free protein is preferred, a construct is currently being synthesized. A similar protein production protocol will still be followed however a tag cleavage protocol will have to be developed and optimized as well. Although crystallography will continue to be pursued, higher resolution electron microscopy may prove to be just as important for structure determination due to the size and complexity of the protein. Future experiments will also include studies with the other homologue of PHB, Prohibitin 2. It will be interesting to observe the interactions between the two homologues and hopefully be included in structure determination experiments as well. Work introduced earlier by Berger *et al* (1998). showed that, in yeast, null mutants of either PHB1 or PHB2 resulted in undetectable levels of the other homologue. [7] This suggests further experiments with both homologues may provide improved structural experiments. The various post-translational modifications mentioned in the introduction may prove to be essential for the stability of PHB when it comes to structure determination. Since these modifications are not very common in usual prokaryotic culture systems, eukaryotic cells might be considered for future protein expression. [60] Many of the experiments that involve function determination of PHB involve yeast cultures for protein expression. PHB is an active target for many drugs such as flavaglines, a natural product extracted from *Aglaia* plants. [61] Future experiments to study structural interactions between the protein and drugs may be of interest in understanding drug activity and function.

6.0 CONCLUSIONS

PHB1 is a very interesting protein for structural studies due to it's large complex structure and wide range of functions and interactions. Protein structure determination requires fairly large amounts of pure protein. Most of the time spent on this project went into optimizing purification protocols for protein quality and yield. Through the use of inclusion bodies, protein denaturation, and renaturation a construct of (PHB1)-25-252-CHis$_6$ was successfully produced in sufficient yields for several structural and biophysical experiments. The experiments suggest the protein exists in large complexes composed of a large number of (PHB1)-25-252-CHis$_6$ monomers. DLS and AUC experiments show an irregular trend such that as the protein concentration increases, the protein hydrodynamic radius and density decreases. This observation would be contrary to what is expected for other proteins. Although experiments were conducted on a protein with an intact affinity tag, the results still provide insights into the next steps required for determining the structure of PHB1 with the possible inclusion of electron microscopy.

6.0 REFERENCES

[1] - McClung, J. K., Danner, D. B., Stewart, D. a, Smith, J. R., Schneider, E. L., Lumpkin, C. K., Nuell, M. J. (1989). Isolation of a cDNA that hybrid selects antiproliferative mRNA from rat liver. *Biochemical and Biophysical Research Communications*, *164*(3), 1316–1322.

[2] - Jupe, E. R., Liu, X., Kiehlbauch, J. L., McClung, J. K., & Orco, R. T. D. (1996). Prohibitin in Breast Cancer Cell Lines: Loss of Antiproliferative Activity Is Linked to 3' Untranslated Region Mutations1, *7*, 871–878.

[3] - Thuaud, F., Ribeiro, N., Nebigil, C. G., & Désaubry, L. (2013). Prohibitin ligands in cell death and survival: Mode of action and therapeutic potential. *Chemistry and Biology*, *20*(3), 316–331.

[4] - Osman, C., Merkwirth, C., & Langer, T. (2009). Prohibitins and the functional compartmentalization of mitochondrial membranes. *Journal of Cell Science, 122,* 3823-3830

[5] - Winter, A., Kämäräinen, O., & Hofmann, A. (2007). Molecular modeling of prohibitin domains. *Proteins: Structure, Function and Genetics*, *68*(1), 353–362.

[6] - Merkwirth, C., & Langer, T. (2009). Prohibitin function within mitochondria: Essential roles for cell proliferation and cristae morphogenesis. *Biochimica et Biophysica Acta - Molecular Cell Research*, *1793*(1), 27–32.

[7] - Berger, K. H., & Yaffe, M. P. (1998). Prohibitin family members interact genetically with mitochondrial inheritance components in Saccharomyces cerevisiae. *Molecular and Cellular Biology*, *18*(7), 4043–52.

[8] - Back, J. W., Sanz, M. A., De Jong, L., De Koning, L. J., Nijtmans, L. G. J., De Koster, C. G., Muijsers, A. O. (2002). A structure for the yeast prohibitin complex: Structure prediction and evidence from chemical crosslinking and mass spectrometry. *Protein Science: A Publication of the Protein Society*, *11*(10), 2471–2478.

[9] - Tatsuta, T., Model, K., Langer, T. (2005). Formation of membrane-bound ring complexes by prohibitins in mitochondria. *Molecular Biology of the Cell, 16*, 248–259.

[10] - Tanaka, H., Kato, K., Yamashita, E., Sumizawa, T., Zhou, Y., Yao, M., Tsukihara, T. (2009). The structure of rat liver vault at 3.5 angstrom resolution. *Science (New York, N.Y.)*, *323*(5912), 384–388.

[11] - Steglich, G., Neupert, W., & Langer, T. (1999). Prohibitins regulate membrane protein degradation by the m-AAA protease in mitochondria. *Molecular and Cellular Biology*, *19*(5), 3435–3442.

[12] - Nijtmans, L. G., de Jong, L., Artal Sanz, M., Coates, P. J., Berden, J. a, Back, J. W., Grivell, L. A. (2000). Prohibitins act as a membrane-bound chaperone for the stabilization of mitochondrial proteins. *The EMBO Journal*, *19*(11), 2444–2451.

[13] - Kasashima, K., Sumitani, M., Satoh, M., & Endo, H. (2008). Human prohibitin 1 maintains the organization and stability of the mitochondrial nucleoids. *Experimental Cell Research*, *314*(5), 988–996.

[14] - Nelson, D. L., Cox, M. M. (2008) *Principles of Biochemistry (5th ed.)*. NewYork, NY: W.H. Freman and Company

[15] - Mishra, S., Ande, S. R., & Nyomba, B. L. G. (2010). The role of prohibitin in cell signaling. *FEBS Journal*, *277*(19), 3937–3946.

[16] - Ande, S. R., & Mishra, S. (2009). Prohibitin interacts with phosphatidylinositol 3,4,5-triphosphate (PIP3) and modulates insulin signaling. *Biochemical and Biophysical Research Communications*, *390*(3), 1023–1028.

[17] - Ande, S. R., Gu, Y., Nyomba, B. L. G., & Mishra, S. (2009). Insulin induced phosphorylation of prohibitin at tyrosine114 recruits Shp1. *Biochimica et Biophysica Acta - Molecular Cell Research*, *1793*(8), 1372–1378.

[18] - Peng, Y.-T., Chen, P., Ouyang, R.-Y., & Song, L. (2015). Multifaceted role of prohibitin in cell survival and apoptosis. *Apoptosis*, *20*(9), 1135–1149.

[19] - Chiu, C., Ho, M., Peng, J., Hung, S., Lee, W., Liang, C. M., & Liang, S. (2012). Raf activation by Ras and promotion of cellular metastasis require phosphorylation of prohibitin in the raft domain of the plasma membrane. *Oncogene*, 32, 777-787.

[20] - Ande, S. R., & Mishra, S. (2011). Nuclear coded mitochondrial protein prohibitin is an iron regulated iron binding protein. *Mitochondrion*, *11*(1), 40–47.

[21] - Resh, M. D. (1996). Regulation of cellular signalling by fatty acid acylation and prenylation of signal transduction proteins. *Cellular Signalling*, *8*(6), 403–412.

[22] - Resh, M. D. (1999). Fatty acylation of proteins: New insights into membrane targeting of myristoylated and palmitoylated proteins. *Biochimica et Biophysica Acta - Molecular Cell Research*, *1451*(1), 1–16.

[23] - Ande, S. R., & Mishra, S. (2010). Palmitoylation of prohibitin at cysteine 69 facilitates its membrane translocation and interaction with Eps 15 homology domain protein 2 (EHD2). *Biochemistry and Cell Biology*, *88*(3), 553–558.

[24] - Korade, Z., & Kenworthy, A. K. (2008). Lipid rafts, cholesterol, and the brain. *Neuropharmacology*, *55*(8), 1265–1273.

[25] - Morrow, I. C., & Parton, R. G. (2005). Flotillins and the PHB domain protein family: Rafts worms and anaesthetics. *Traffic*, *6*(9), 725–740.

[26] - Nadimpalli, R., Yalpani, N., Johal, G. S., & Simmons, C. R. (2000). Prohibitins, stomatins, and plant disease response genes compose a protein superfamily that controls cell proliferation, ion channel regulation, and death. *Journal of Biological Chemistry*, *275*(38), 29579–29586.

[27] - Ahn, C. S., Lee, J. H., Reum Hwang, A., Kim, W. T., & Pai, H. S. (2006). Prohibitin is involved in mitochondrial biogenesis in plants. *Plant Journal*, *46*(4), 658–667.

[28] - Sanz, M. A., Tsang, W. Y., Willems, E. M., Grivell, L. A., Lemire, B. D., Van der Spek, H., & Nijtmans, L. G. J. (2003). The mitochondrial prohibitin complex is essential for embryonic viability and germline function in Caenorhabditis elegans. *Journal of Biological Chemistry*, *278*(34), 32091–32099.

[29] - Singh, A., Upadhyay, V., & Panda, A. K. (2014). Solubilization and refolding of inclusion body proteins. *Insoluble Proteins: Methods and Protocols*, *99*(4), 283–291.

[30] - Das, A., & Mukhopadhyay, C. (2009). Urea-mediated protein denaturation: a consensus view. *The Journal of Physical Chemistry. B*, *113*(38), 12816–24.

[31] - Palmer, I., & Wingfield, P. T. (2012). Preparation and Extraction of Insoluble (Inclusion-Body) Proteins from *Escherichia coli*. *NIH Public Access*, (8 M), 1–25.

[32] - Lorber, B., Fischer, F., Bailly, M., Roy, H., & Kern, D. (2012). Protein analysis by dynamic light scattering: Methods and techniques for students. *Biochemistry and Molecular Biology Education*, *40*(6), 372–382.

[33] - Arzenšek, D., Podgornik, R., & Kuzman, D. (2010). Dynamic light scattering and application to proteins in solutions. *Seminar, Department of Physics, University of Ljubljana*, 1–18. Retrieved from: http://mafija.fmf.unilj.si/seminar/files/2009_2010/Dynamic_light_scattering_and_application_to_proteins_in_solutions.pdf

[34] - Ferré-D'Amaré, A. R., & Burley, S. K. (1994). Use of dynamic light scattering to assess crystallizability of macromolecules and macromolecular assemblies. *Structure (London, England: 1993)*, *2*(5), 357–359.

[35] - Cole, J. L., Lary, J. W., Moody, T., & Laue, T. M. (2009). Analytical Ultracentrifugation: Sedimentation Velocity and Sedimentation Equilibrium. *Methods of Cell Biology*, *84*(07), 1433–179.

[36] - Lebowitz, J., Lewis, M. S., & Schuck, P. (2002). Modern analytical ultracentrifugation in protein science: a tutorial review. *Protein Science: A Publication of the Protein Society*, *11*(9), 2067–2079.

[37] - Lipfert, J., & Doniach, S. (2007). Small-angle X-ray scattering from RNA, proteins, and protein complexes. *Annual Review of Biophysics and Biomolecular Structure*, *36*, 307–327.

[38] - Mertens, H. D. T., & Svergun, D. I. (2010). Structural characterization of proteins and complexes using small-angle X-ray solution scattering. *Journal of Structural Biology*, *172*(1), 128–141.

[39] - Sreerama, N. and Woody, R.W. (2000) Estimation of protein secondary structure from CD spectra: Comparison of CONTIN, SELCON and CDSSTR methods with an expanded reference set. *Anal. Biochem. 287(2)*, 252-260.

[40] - Sen, T. Z., Jernigan, R. L., Garnier, J., & Kloczkowski, A. (2005). GORIV server for protein secondary structure prediction. *Bioinformatics*, *21*(11), 2787–2788.

[41] - Hurton, T., Wright, A., Deubler, G., & Bashir, B. (2012, August 28). Sedimentation Interpretation Program. Retrieved from http://sednterp.unh.edu/.

[42] - Laue, T. M., Shah, B. D., Ridgeway, T. M., Pelletier, S. L. (1992). Analytical Ultracentrifugation in Biochemistry and Polymer Science, Royal Society of Chemistry (Edited by S. Harding and A. Rowe), 90-125.

[43] - Schuck, P. (2000). Size-distribution analysis of macromolecules by sedimentation velocity ultracentrifugation and lamm equation modeling. *Biophysical Journal*, *78*(3), 1606–1619.

[44] - Rambo, R. P. (n.d.). BIOSIS. Retrieved from http://www.bioisis.net/welcome.

[45] - Konarev, P. V., Volkov, V. V., Sokolova, A. V., Koch, M. H. J., Svergun, D. I. (2003). PRIMUS - a Windows-PC based system for small-angle scattering data analysis. *Journal of Applied Crystallography*. 36, 1277-1282.

[46] - Franke, D. and Svergun, D.I. (2009) DAMMIF, a program for rapid ab-initio shape determination in small-angle scattering. *Journal of Applied Crystallography*, **42**, 342-346.

[47] - Volkov, V. V, and Svergun, D. I. (2003) Uniqueness of ab initio shape determination in small-angle scattering. *Journal of Applied Crystallography*, *36*, 860–864.

[48] - Sørensen, H. P., & Mortensen, K. K. (2005). Soluble expression of recombinant proteins in the cytoplasm of Escherichia coli. *Microbial Cell Factories*, *4*(1), 1.

[49] - Chesshyre, J. A., Hipkiss, A. R. (1989). Low temperatures stabilize interferon α-2 against proteolysis in *Methylophilus methylotrophus* and *Escherichia coli. Applied Microbiology and Biotechnology, 31*, 158-162.

[50] - Mitraki, A, Betton, J. M., Desmadril, M., & Yon, J. M. (1987). Quasi-irreversibility in the unfolding-refolding transition of phosphoglycerate kinase induced by guanidine hydrochloride. *European Journal of Biochemistry / FEBS*, *163*(1), 29–34.

[51] - Némethy, G., & Scheraga, H. A. (1962). the Structure of Water and Hydrophobic Bonding in Proteins. Iii. the Thermodynamic Properties of Hydrophobic Bonds in Proteins1, 2. *The Journal of Physical Chemistry*, *66*(10), 1773–1789.

[52] - Kiefhaber, T., Rudolph, R., Kohler, H. H., & Buchner, J. (1991). Protein aggregation in vitro and in vivo: a quantitative model of the kinetic competition between folding and aggregation. *Biotechnology (Nature Publishing Company)*, *9*(9), 825–829.

[53] - Hong, P., Koza, S., & Bouvier, E. S. P. (2012). Size-Exclusion Chromatography for the Analysis of Protein Biotherapeutics and their Aggregates. *Journal of Liquid Chromatography & Related Technologies*, *35*(20), 2923–2950.

[54] - Song, B., Cho, J. H., & Raleigh, D. P. (2007). Ionic-strength-dependent effects in protein folding: Analysis of rate equilibrium free-energy relationships and their interpretation. *Biochemistry*, *46*(49), 14206–14214.

[55] - Duong-Ly, K. C., & Gabelli, S. B. (2014). *Salting out of proteins using ammonium sulfate precipitation*. *Methods in Enzymology* (1st ed., Vol. 541). Elsevier Inc.

[56] - Putnam, C. D., Hammel, M., Hura, G. L., & Tainer, J. a. (2007). X-ray solution scattering (SAXS) combined with crystallography and computation: defining accurate macromolecular structures, conformations and assemblies in solution. *Quarterly Reviews of Biophysics*, *40*(3), 191–285.

[57] - Carson, M., Johnson, D. H., McDonald, H., Brouillette, C., DeLucas, L. J. (2007) His-tag impact on structure. *Acta Crystallographica Section D Biological Crystallography, 63*, 295-301

[58] - Zhou, X., Zhao, G., Truglio, J. J., Wang, L., Li, G., Lennarz, W. J., & Schindelin, H. (2006). Structural and biochemical studies of the C-terminal domain of mouse peptide-N-glycanase identify it as a mannose-binding module. *Proceedings of the National Academy of Sciences of the United States of America*, *103*(46), 17214–9.

[59] - Habe, H., Morii, K., Fushinobu, S., Nam, J. W., Ayabe, Y., Yoshida, T., Omori, T. (2003). Crystal structure of a histidine-tagged serine hydrolase involved in the carbazole degradation (CarC enzyme). *Biochemical and Biophysical Research Communications*, *303*(2), 631–639.

[60] - Dell, A., Galadari, A., Sastre, F., & Hitchen, P. (2010). Similarities and differences in the glycosylation mechanisms in prokaryotes and eukaryotes. *International Journal of Microbiology, 2010*.

[61] - Polier, G., Neumann, J., Thuaud, F., Ribeiro, N., Gelhaus, C., Schmidt, H., Li-Weber, M. (2012). The natural anticancer compounds rocaglamides inhibit the Raf-MEK-ERK pathway by targeting prohibitin 1 and 2. *Chemistry and Biology, 19*(9), 1093–1104.